

THESIS

EFFECTIVE PROPERTIES OF MAGNETO-ELECTRO-ELASTIC TWO-DIMENSIONAL CELLULAR SOLIDS

Submitted by

Mustafa M. Khattab

Department of Civil and Environmental Engineering

In partial fulfillment of the requirements

For the Degree of Master of Science

Colorado State University

Fort Collins, Colorado

Spring 2016

Master's Committee:

Advisor: Paul Heyliger

Bruce Ellingwood

Christian Puttlitz

Copyright by Mustafa Khattab 2016

All Rights Reserved

## ABSTRACT

### EFFECTIVE PROPERTIES OF MAGNETO-ELECTRO-ELASTIC TWO-DIMENSIONAL CELLULAR SOLIDS

Two-dimensional cellular solids composed of magneto-electro-elastic (MEE) materials were studied using the finite element method (FEM). A MATLAB code was written to implement field models to determine the effective properties for this cellular solid including elastic, piezoelectric, piezomagnetic, thermal, pyroelectric and pyromagnetic effective properties as a function of the relative density. Results obtained for purely elastic properties were compared with results from other studies and showed good agreement. Varying microstructures of the cellular solids including square, equilateral triangle and hexagonal systems, were considered and comparisons between the results of all the geometries were established. The triangular cellular solid was the stiffest among all shapes, and the regular hexagon cellular solid showed the highest effective coupling constants for the piezoelectric, piezomagnetic, pyroelectric and pyromagnetic coefficients. The thermal expansion coefficient was found to be independent from the relative density and was constant for all the MEE cellular solid shapes. A set of simple equations are proposed to approximate the effective properties for these low density MEE solids.

## ACKNOWLEDGEMENTS

I am grateful to the God who gave me the strength, health and ability to finish the thesis. I would like to thank Prof. Paul Heyliger for his continuous and valuable guidance through the work on this thesis and for his knowledge that he gave me. I also would like to thank my committee members Prof. Bruce Ellingwood and Prof. Christian Puttlitz. My sincere thanks also goes to Mr. Dher Agha for helping me debug some parts of the code. Special thanks to the government of Iraq for supporting me financially during the time I spent at Colorado State University. Finally, I would like to thank my parents, Brother and Sister for their continuous support. Without them I would never reach this far.

## TABLE OF CONTENTS

ABSTRACT .....	ii
ACKNOWLEDGEMENTS .....	iii
CHAPTER 1: INTRODUCTION .....	1
1.1 Introduction: .....	1
1.2 Objectives:.....	3
1.3 Thesis organization.....	3
CHAPTER 2: LITERATURE REVIEW .....	5
2.1 Background.....	5
2.2 Modeling and mechanics of two-dimensional cellular solids .....	7
2.3.1 Magneto-Electro effect .....	9
2.3.2 Multi-physics of MEE composites .....	12
2.4 Smart material cellular solids.....	14
2.5 Significance of this research.....	15
CHAPTER 3: METHOD.....	16
3.1 Governing Equations: .....	16
3.2 Homogenization .....	18
3.3 Repeating unit cell (RUC) .....	20
3.3 Finite Element Method .....	21
3.3.1 Discretization.....	22
3.3.2 Weak form.....	22
3.3.3 Element matrices.....	26
3.4 Boundary conditions and the effective properties .....	26
3.4.1 Effective elastic properties.....	26
3.4.2 The effective electric and magnetic properties .....	31
3.4.3 The effective thermal expansion and moisture expansion coefficients.....	32
3.4.4 The effective pyroelectric and pyromagnetic coefficients .....	33
3.5 The Relative Density.....	33
3.6 Computational Model .....	34

CHAPTER 4: RESULTS AND DISCUSSION .....	35
4.1 The relative density:.....	35
4.2 The elastic properties:.....	37
4.3 The effective piezoelectric properties: .....	45
4.4 The effective piezomagnetic properties: .....	49
4.5 The thermal expansion coefficient: .....	54
4.6 The effective pyroelectric and pyromagnetic properties: .....	55
4.7 Suggested equations for the effective properties .....	59
CHAPTER 5: SUMMARY AND CONCLUSION .....	64
5.1 Conclusions: .....	64
5.2 Future work: .....	66
REFERENCES .....	67
APPENDIX A: ELEMENTS OF THE MATRIX EQUATIONS FOR THE RITZ MODEL.....	71
APPENDIX B: MATLAB CODE .....	74

# CHAPTER 1: INTRODUCTION

## 1.1 Introduction:

Cellular solids refer to materials that contain numerous cells where the volume between the cell walls is filled by air. The shape of these cells can vary from regular shapes to totally random configurations. Cellular solids are usually classified into two-dimensional cellular solids that are called honeycombs and three-dimensional and more complex structures that are called foams. Several examples are shown in Figure 1.1.

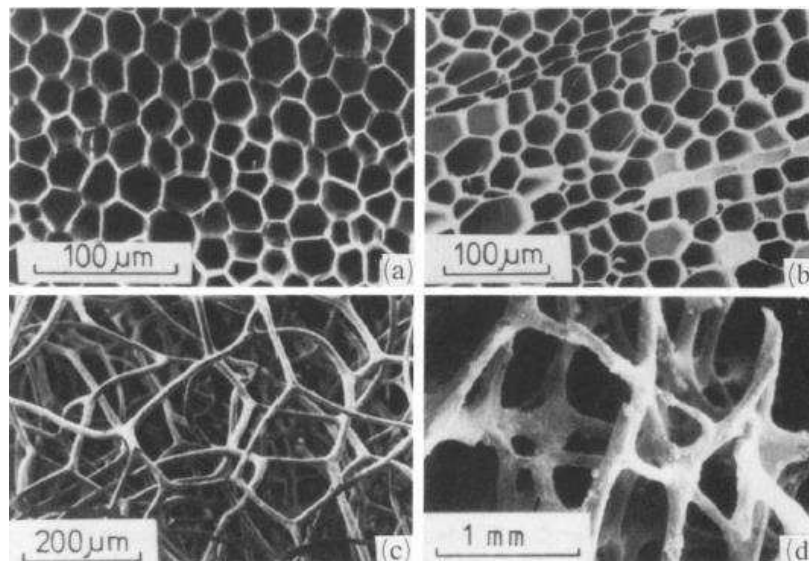


Figure 1.1: Natural cellular solids: (a) cork (b) balsa (c) sponge (d) cancellous bone (Gibson, 1989).

The cell walls of the foams can be either open, partially closed, or closed. Cellular solids can be found in nature and includes material such as wood, cork and bones of the human body or it can be made artificially by different materials (e.g. polymers, metals, ceramics and glass). Recently, man-made cellular solids have gained a special interest because of the benefits of such

materials in light weight structure such as sandwich panels. Some of their benefits include having low densities but relatively high stiffness and strength compared to ordinary solids. They can also be used as an impact absorbers because of their ability to undergo large compressive strains compared with regular solids.

Materials that are made from Magneto-Electro-Elastic (MEE) composites have somewhat different benefits. MEE composites are made from combining piezoelectric materials, which can induce electric field by applying stresses on it and vice versa, and piezomagnetic material, which can induce magnetic field by applying stresses on it and vice versa. These materials have potential product properties that couple these interactions. MEE composites can be used in smart structures, structural health monitoring, green energy and energy harvesting, sound devices, biomedical devices and many increasing applications. Such materials are at present relatively expensive compared to others. Finding some ways to reduce the cost while maintaining its properties is essential in starting using these materials more widely. The technologies of making cellular solids from any material is available as mentioned in Gibson and Ashby (1997) so the benefits of combing the benefits of the two and examine the behavior of cellular solids that are made from MEE composite could be significant.

In this research, two-dimensional cellular solids that are composed of MEE constituents will be studied by finding the effective properties of these cellular solids. Of primary interest is the effect of the cell shapes and the relative density on these properties. These will be studied using finite element models of the full two-dimensional governing equations of the solid. To the author's knowledge, this is the first research to study a MEE cellular solid.

## 1.2 Objectives:

The objectives of this work are to:

- Determine the effective elastic properties for the three shapes of honeycomb and compare the results with existing studies.
- Determine the effective piezoelectric, piezomagnetic properties for the three shapes of honeycomb.
- Determine the effective thermal expansion coefficient for all the shapes.
- Study the temperature effect on the piezoelectric and piezomagnetic properties by finding the pyroelectric and pyromagnetic properties for the honeycombs.
- Study the effect of the relative density of the honeycomb on all the properties.
- Establish comparisons between the three shapes of the honeycomb and find which shape will give the highest values for all the effective properties.
- Suggest a set of relatively simple equations to represent all the effective properties of the MEE cellular solid in terms of the relative density.

## 1.3 Thesis organization

Chapter 1 of this thesis is an introduction that contains necessary background and brief definitions of cellular solids and the smart material (MEE composites) that are used in this study. Chapter 2 gives a review of the literature that has been used to develop a better understanding on the subjects of cellular solids and the MEE composites. The first part of Chapter 2 will discuss the literature on cellular solids while the second part will show the history, applications and the literature on the MEE composites. The third part will mention the existing studies on smart material cellular solids. Chapter 3 will present all the theoretical developments, governing

equations and methods that were used in the study. Chapter 4 contains the results showed in figures and tables and comparison with existing studies are also shown. Discussions and explanations of the results are also provided. Suggested equations for the effective properties can also be found in Chapter 4. Chapter 5 presents the conclusions and all the findings of the study and also will discuss the possible future work and what can be added to improve this study. An Appendix is provided that will show the written MATLAB code and will have the elements of the matrix equations for the Ritz model and other computational details.

## CHAPTER 2: LITERATURE REVIEW

### 2.1 Background

Significant prior work has been published on cellular solids. This is an enormous subject because of the variability of the constituent materials, cell shapes and cell sizes. Cellular solids can be found either in nature (e.g. wood, cork and human bone) or those that are artificially manufactured (e.g. polymeric foams used for impact absorption). There is significant variety in the studies that depend on how those foams are used or how they are made. In practice, foams are any solid that have a relative density that is less than (0.3). A solid have a relative density that is greater than (0.3) can be considered as a solid with isolated pores [Gibson & Ashby, 1997].

One of the most important summaries of cellular solids is that of Gibson and Ashby (1997). This work has been referenced in for almost every study that has been done on cellular solids. It covers a vast subjects discussing the mechanical, thermal, electrical and acoustic properties of cellular solids and foams. Cellular solids are classified into honeycombs, which implies a two dimensional cellular solid with triangular, square or hexagonal cells, and foams, which refers to a three dimensional and more complicated version of cellular solids. Foams can be open celled or partially closed and fully closed, each of which can affect its properties significantly. This research will focus on two-dimensional cellular materials composed of materials that couple elastic, electric, and magnetic fields.

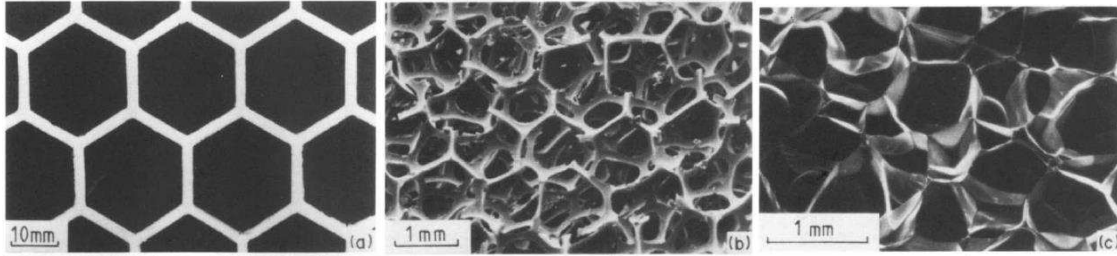


Figure 2.1: Cellular solids (a) Honeycomb; (b) open-cell foam; (c) closed-cell foam (Gibson, 1989)

One important property of cellular solids is the relative density. This is easily-calculated parameter that gives the portion of volume that is occupied by material. It has been shown that many of the mechanical properties of cellular solids can be related to its relative density in the form of:

$$\frac{\phi^*}{\phi_s} = c \left( \frac{\rho^*}{\rho_s} \right)^p \quad 2.1$$

Where:

$\phi^*$ : Any effective mechanical property for the foam.

$\phi_s$ : Any mechanical property for the constituent solid.

$\frac{\rho^*}{\rho_s}$ : The relative density of the foam.

c and p: Constants depend on the microstructure of the foam

Researchers have studied the behavior of cellular solids under the effect of high temperature and the effect of moisture on foams especially for sandwich panels and wood. The work on piezoelectric, piezomagnetic and magneto-electro-elastic cellular solids is somewhat limited.

## 2.2 Modeling and mechanics of two-dimensional cellular solids

Significant effort has been devoted to the study of cellular solids, and the literature on cellular solids shows a variety of approaches. Early researchers studied a representative unit cell assuming that the cellular solid is periodic and generally not taking into account any irregularities in the cells. Gibson et al. (1982) studied the plane properties of honeycomb when loaded in  $X_1$  and  $X_2$  directions, as can be seen in Figure 2.2, experimentally and theoretically. They found a relationship between the relative density and the thickness  $t$  and the length  $l$  of the cell wall for the regular hexagonal honeycomb ( $\theta=30$ ) that can be shown as:

$$\frac{\rho^*}{\rho_s} = \frac{2}{\sqrt{3}} \frac{t}{l} \quad 2.2$$

Gibson and co-workers (1982) carried out an experimental work on honeycomb with different cell dimensions and found the elastic properties of the honeycomb. Theoretically, they found a relationships between the elastic properties of the honeycomb and the cell dimensions ( $t$ ,  $l$  and  $\theta$ ), Figure 2.2, by assuming the cell wall will behave as a simple beam where bending of the cell wall acts as the main deformation mode. The theoretical and the experimental work showed good agreement. Warren and Kraynik (1987) used a different approach to study the elastic response of periodic two-dimensional cellular materials by studying different repeating volumes consisting from three elements connected at a node. They considered axial and shear deformation in their analyses in addition to bending deformation. They found an expressions for the elastic properties and found that for low-density honeycomb the effective properties can be determined by the bending mechanism.

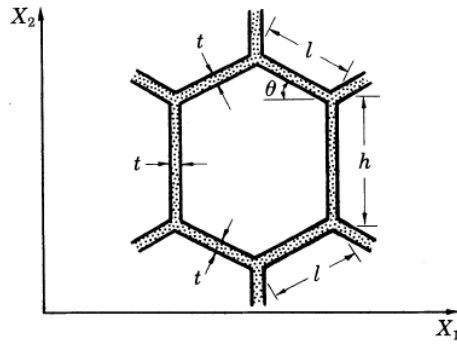


Figure 2.2: Two-dimensional Hexagonal Unit cell (Gibson et al., 1982)

Christensen (2000) studied different shapes of two-dimensional low density cells (triangular, hexagonal, triangular and hexagonal, hexagonal and stars) and found the expression for the elastic properties in term of the volume fraction of material  $(1-c)$  when  $c$  is volume fraction of the voids and  $(1-c)$  is equal to the relative density  $(\frac{\rho^*}{\rho_s})$ . For the effective modulus of elasticity, all the cell shapes have the expression of  $(1 - c)^3$  because of the bending in the cell walls. The triangular cells have the expression  $(1 - c)$  because they act like a truss. For example:

$$\text{For triangular cell:} \quad \frac{E}{E_m} = \frac{1}{3} (1 - c) \quad 2.3$$

$$\text{For hexagonal cell:} \quad \frac{E}{E_m} = \frac{3}{2} (1 - c)^3 \quad 2.4$$

Hohe and Becker (2003) studied a periodic two-dimensional hexagonal honeycomb made from hyperelastic material and found the effective stress-strain when uniaxial, biaxial and shear loading are applied. They studied a repeating unit cell (RUC) similar to that studied by Warren and Kraynik (1987). They found that the behavior of cellular solid under infinitesimal strain will

be different from its behavior under finite strain. Cell wall alignment can play a role in this behavior since its effect can be neglected for infinitesimal strains and it can cause anisotropies under large strains even for initially isotropic cellular solid.

In practice, it is difficult to find a periodic cellular solid without any defects or irregularities. Many manmade or natural foams possess a random microstructure. For this reason, the effect of irregularities and defects on the behavior of cellular solids have seen significant investigation. Silva et al. (1995) investigated the effect of non-periodicity on the elastic properties of foams using the Voronoi method to generate a random cell shapes. The cell walls were analyzed as a 3-node beam using Finite Element Method (ABAQUS software). The cell walls were assumed to be uniform. Silva and Gibson (1997) studied the effect of non-periodicity on the strength of the honeycomb using the same method used in their previous research. Steadman et al. (2014) studied the effect of different irregularities and defects of two-dimensional cellular solid on the elastic properties. They studied the elongation and the shortening of the cell walls, randomly broken cell walls and the effect of thickness variation in the cell walls. They concluded that broken cell walls can cause a significant drop in the elastic properties even with low number of broken cell walls. They also found that cell wall elongation causes anisotropy and the effect of thickness variation can be neglected. This research will only consider a regular two-dimensional cellular solid with no defects or irregularities.

### 2.3.1 Magneto-Electro effect

The first person to study magnetoelectric (ME) material was the French physicist Pierre Curie (1894). Landau and Lifshitz (1957) and Astrov (1960) did experimental work confirming that there can be an electric field generated after applying a magnetic field. All the previous work was

conducted to study a single-phase material like ( $Cr_2O_3$ ). These previous studies indicates that the ME effect in single phase materials can be found only in very low temperatures and the effect is weak such that it is challenging to use in any realistic application.

Suchtelen (1972) proposed a new way to have the ME effect by making a product of composite made from piezoelectric and piezomagnetic materials. This was the first time that MEE composites had been proposed. According to Sun and Kim (2010), MEE composites are made from piezoelectric(e.g., barium titanate , $BaTiO_3$ ) and piezomagnetic (e.g., cobalt iron oxide, $CoFe_2O_4$ ) materials. Individually these have the same properties of its original materials but together possess ME coupling. By applying a magnetic field to the composite, a change in the piezomagnetic material dimensions. Because of the interaction of the materials in the composite, the strain will affect the piezoelectric phase inducing an electric field. The same effect will occur if an electric field has been applied instead of the magnetic field. Magnetoelastic (MEE) composites can be made by making one of the materials as a matrix and the other is embedded in the matrix in the form of particles, fibers or by making a multiple layers of these materials. The latter is the most common way to construct these solids because of the ease of fabrication.

Van Run et al. (1974) found the properties of (barium titanate)-(Cobalt ferrite-titanate) composite by experimental work. Van Boomgaard and Born (1978) conducted a series of experiments to study the first particulate (0-3, 3-0) ME composite, and they found the optimal ratio of the composite material that gives the strongest ME coupling. The work that has been done in the 1970's and the 1980's was nearly all experimental.

Harshe et al. (1993) were the first to develop a theoretical solution for a particulate ME composite (0-3, 3-0) by modeling the composite with simple small cubes. They compared their results with earlier experimental work. The numbers (0-3, 3-0) means that one of the materials is continuous in three directions (3) and the other is in the form of particles (0). For the (1-3), the number (1) means that the composite is fibrous that one of the materials is continues in one direction. The (2-2) ME composite means both materials are continuous in 2 directions such as the multi layered ME composite.

Nan (1994) tried a different approach from Harshe et al. (1993) to study the ME effect by developing a theoretical approach to find the effective ME coefficients of the (1-3) and (3-1) composites made from  $BaTiO_3-CoFe_2O_4$  using Green's Function method. This method showed a good agreement with experimental results from previous work.

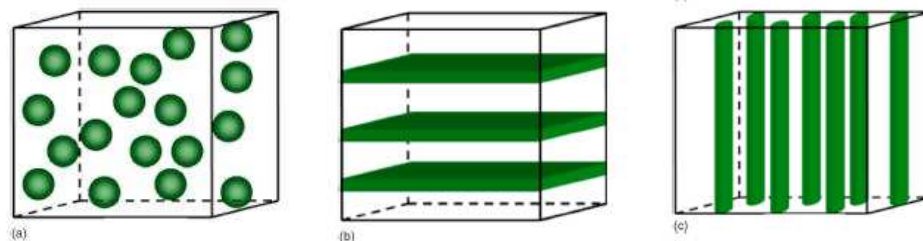


Figure 2.2: Types of MEE composites (a) (0-3) particulate composite, (b) (2-2) Laminate composite and (c) (1-3) Fibrous composite (Nan et al., 2008)

Li and Dunn (1998) developed a micromechanical method to find the effective MEE coefficients using the Mori-Tanaka (mean field) method (1973). They found an exact relations for the effective magneto-elastic moduli.

MEE laminated plate (2-2) composites have seen significant study. Pan (2001) found the exact solution for displacements, stress, electric potential and magnetic potential in a three-dimensional multilayered MEE plates under the effect of static surface and internal stress. Pan and Heyliger (2002) studied the free vibration of MEE plates with simply supported boundary conditions on all of its edges. By finding the natural frequencies and the mode shapes, they observed that some of the modes do not produce any electric or magnetic potentials and these modes are purely elastic. Ramirez et al. (2006) have developed an approximate method to find the solution for the free vibration of MEE laminates and compared the results to the exact solution and to the result obtained from FE analysis using ABAQUS. The results showed a good agreement. Additional literature surveys can be found in the review papers of Nan et al. (2008) and Kambale et al. (2012).

### 2.3.2 Multi-physics of MEE composites

Nan (1994) was among the first researchers to study the Thermo-Electro-Elastic coupling of a piezoelectric composite. A (0-3) composite made from epoxy as the matrix and reinforced by  $BaTiO_3$  particles. The product pyroelectricity coefficient, the coupled coefficient of thermal expansion and piezoelectricity, of the composite were all found but the pyroelectricity of the  $BaTiO_3$  was ignored and only the generated electrical polarization in the piezoelectric phase

due to stress caused by the difference in thermal coefficients of the two phases when the temperature is increased in the matrix material was studied.

Aboudi (2001) studied Electro-Magneto-Thermo-Elastic (1-3) composite and predicted the effective elastic, thermal expansion, piezoelectric, piezomagnetic, pyroelectric and pyromagnetic coefficients using a homogenization micromechanical method. A repeating unit cell assuming that the composite is periodic. Results were compared to the Mori-Tanaka method and showed a good agreement.

Zhang and Wang (2015) studied Magneto-Electro-Thermo-elastic coupling of fibrous (1-3) composites using the Finite Element Method. They also found the effective properties of the product composite by taking a representative Volume Element (RVE) and apply the homogenization approximation. They compared some of the results with the Mori-Tanaka Method to validate their results.

Adding more fields to the ME coupling was the point of interest in the last two decades. Smittakorn and Heyliger (2000) studied the effect of temperature and moisture on the steady-state and transient behavior of laminated piezoelectric plates by applying the boundary conditions on the top and the bottom of the plate. Recently, there was a significant increase of work completed on the multi-physics of functionally graded materials (FGM) like the work done by Akbarzadeh and Chen (2012) and the work by Zenkour (2014). Akbarzadeh and Pasini (2014) were the first to study all the fields coupled together. They studied the hygro-thermo-magneto-electro-elastic coupling of multilayered and functionally graded with hollow or solid cross-section and infinitely long cylinders, finding the exact solution for every field in the layers of FG cylinders.

## 2.4 Smart material cellular solids

Most of the work that has been done on cellular solids focused on the mechanical behavior. Moreover, the mechanical, thermal, electrical, and the acoustic properties have been found for different types of cellular solids. However, little work has been completed on the foams that are made from smart materials (piezoelectric or piezomagnetic materials).

Dunn and Taya (1993) were the first to study a piezoelectric material with pores. They studied the effect of porosity volume fraction on the elastic, dielectric and the electro-elastic moduli for different types of piezoelectric ceramics. A closer look at the results indicates that a decrease in these moduli with the increase of the porosity volume fraction. Iyer and Venkatesh (2014) performed an analysis on a periodic (0-3) and (1-3) piezoelectric composite that contains pores using the homogenization method. They found the electromechanical properties and the effect of the pores sizes and the shape. Their results showed a good agreement with the results from Dunn and Taya (1993). The dielectric and the piezoelectric constants decreased when the porosity volume fraction was increased. These solids are not honeycombs or foams but do have the likelihood of relatively low density.

Huang et al. (2009) studied the effect of ellipsoidal voids on the effective properties of the Magneto-electroelastic (MEE) composites. Finding the effect of the void volume fraction and the orientation of the voids on the effective piezomagnetic, piezoelectric and magneoelectric properties of the composite.

Challagulla and Venkatesh (2012) conducted a research to study a foam made from piezoelectric material (PZT-7A). They found the elastic, piezoelectric and acoustic properties as a function of the relative density of the foam for a different shapes of unit cells and compared the

results of these different cell shapes using Finite Element modeling software (ABAQUS). Finally, Iyer et al. (2014) studied a honeycomb foam made from piezoelectric material. Again, they found the elastic, dielectric and piezoelectric constants for longitudinally and transversely porous foams for a different shapes of unit cells (rectangular and Hexagonal) in terms of the relative density of the foam. The unit cell analysis was carried by the finite element analysis software (ABAQUS). There is no work that has been done on adding more fields to the piezoelectric cellular solids nor any work on a cellular solid made from MEE composite.

## 2.5 Significance of this research

Two-dimensional cellular solids made from MEE composite are considered to find the effective properties including the elastic and the thermal coefficients and the effective coupled coefficients including the thermal expansion, pyroelectric and the pyromagnetic coefficients for different shapes of unit cell of the cellular solid and compare the results. The Finite Element Method (FEM) will be used in this study by a program written in MATLAB. Results will be compared with existing studies, and new results will be presented for several new configurations or loadings.

## CHAPTER 3: METHOD

This chapter will present all the governing equations, theoretical developments and methods that were used in the study.

### 3.1 Governing Equations:

The equations of equilibrium in rectangular Cartesian coordinates can be expressed in indicial form as:

$$\sigma_{ij,j} + f_i = 0 \quad (3.1)$$

Here  $\sigma_{ij}$  are the components of stress and  $f_i$  are the body forces

$i, j$  refer to the directions  $X_1$  and  $X_2$

The quasi-static Maxwell equations in the absence of electric and magnetic sources are given in terms of the components of electric displacement  $D_j$  and magnetic induction  $B_j$  as

$$D_{i,j} = 0 \quad (3.2)$$

$$B_{i,j} = 0 \quad (3.3)$$

The constitutive equations for the class of solid considered in this study are given by:

$$\sigma_{ij} = C_{ijkl}S_{kl} - e_{mij}E_m - d_{mij}H_m - \beta_{ij}\theta - \zeta_{ij}m \quad (3.4)$$

$$D_m = e_{mij}S_{ij} + \epsilon_{mn}E_n + g_{mn}H_n + \gamma_m\theta + X_m m \quad (3.5)$$

$$B_m = d_{mij}S_{ij} + g_{mn}E_n + \mu_{mn}H_n + \tau_m\theta + v_m m \quad (3.6)$$

Where:  $E_m, H_n, C_{ijkl}, e_{mij}, d_{mij}, \epsilon_{mn}, g_{mn}, \mu_{mn}, \beta_{ij}, \zeta_{ij}, \gamma_m, X_m, \tau_m$  and  $v_m$  are the electric field, magnetic field and elastic, piezoelectric, piezomagnetic, dielectric, electromagnetic, magnetic permeability, thermal stress, and hygroscopic stress coefficient tensors and pyroelectric, hygroelectric, pyromagnetic, and hygromagnetic coefficients vectors respectively. Here  $\theta$  and  $m$  represents the change in temperature and change in moisture content respectively.

The strain-displacement relations can be written in RCC assuming small displacement theory as:

$$\begin{aligned} S_{xx} &= \frac{\partial u}{\partial x} \\ S_{yy} &= \frac{\partial v}{\partial y} \end{aligned} \quad (3.7)$$

$$S_{xy} = \frac{\partial v}{\partial x} + \frac{\partial u}{\partial y}$$

Here  $S_{xx}$  and  $S_{yy}$  are the components of the linear normal strain tensor, and  $S_{xy}$  are the engineering shear strain. Here  $x, y$  refer to directions  $X_1$  and  $X_2$ . The electric field components  $E_i$  are related to the electrostatic potential  $\phi(x_1, x_2)$  using the relations:

$$E_i = \frac{\partial \phi}{\partial x_i} \quad (3.8)$$

Similarly, the magnetic induction components  $B_i$  are related to the magnetic potential  $\Psi$  ( $x_1, x_2$ ) using the relations:

$$B_i = \frac{\partial \Psi}{\partial x_i} \quad (3.9)$$

### 3.2 Homogenization

The method of homogenization have been extensively used for composites. The main idea of the homogenization is that to divide total solid into small elements such as the repeating unit cell (RUC) elements or the representative volume element (RVE) and find the effective properties, the product properties of the composite, for the RUC or the RVE and apply it to the whole material assuming that the composite material is a homogenous material with effective properties that have been found for the small element.

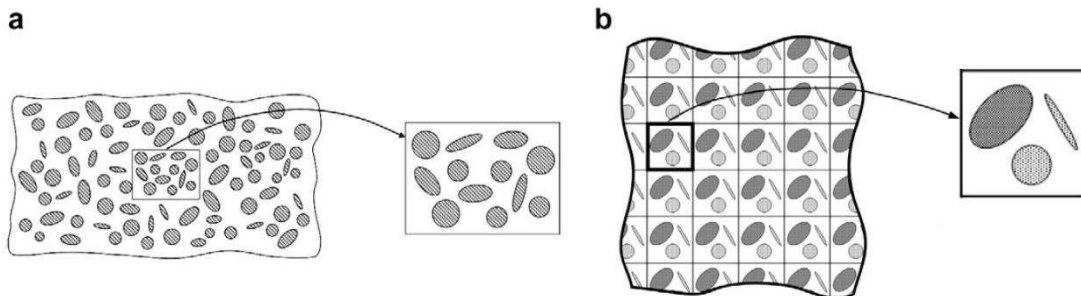


Figure 3.1: Representation of material microstructure. (a) Statistically homogenous material characterized by RVE (b) Periodic microstructure characterized by RUC. (Pindera et al., 2009)

This method allows the determination of the responses of the composite to any applied loads. According to Pindera et al (2009), the representative volume element (RVE) can be used for materials with statistical homogeneity, while the repeating unit cell (RUC) can be used when having a material with periodic structure. In the same way, homogenization can be applied to the cellular solids considered in this study by assuming that it is made from a solid material with no voids that has effective properties as can be seen in Hohe and Becker (2003). In this research the idea of homogenization will be applied twice: once for the MEE composite and the second time for the cellular solid to get its effective properties. The effective properties for the MEE material that are made of 50%  $BaTiO_3$  (piezoelectric material) and 50%  $CoFe_2O_4$  (piezomagnetic material) are taken from Chen et al (2015) and Akbarzadeh and Pasini (2014). They are summarized in Table 1.

Table 1. The effective properties for a composite made of 50%  $BaTiO_3$  and 50%  $CoFe_2O_4$  ( $c_{ij}$  in  $10^9$  N/m<sup>2</sup>,  $e_{ij}$  in C/m<sup>2</sup>,  $d_{ij}$  in N/Am,  $\epsilon_{ij}$  in  $10^{-9}$  C<sup>2</sup>/Nm<sup>2</sup>,  $\mu_{ij}$  in  $10^{-6}$  Ns<sup>2</sup>/C<sup>2</sup>,  $\beta_i$  in N/m<sup>2</sup>K,  $K^t$  in N/sK).

properties	MEE	Properties	MEE	Properties	MEE
c11	213	e22	8.86	$\mu_{11}$	201
c12	113	d11	292	$\mu_{22}$	201
c22	213	d12	222	$\beta_1$	6.105
c66	50	d22	292	$\beta_2$	6.295
e11	8.86	$\epsilon_{11}$	0.24	Kt	0.383
e12	-2.71	$\epsilon_{22}$	0.24		

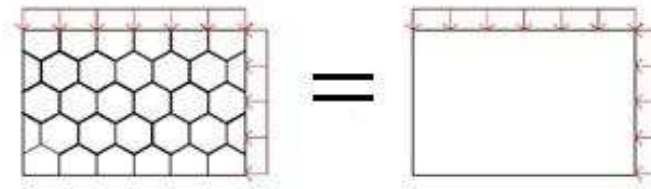
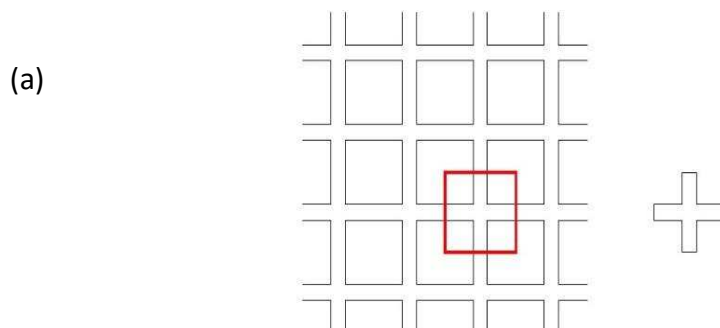


Figure 3.2: Homogenization of cellular solids

### 3.3 Repeating unit cell (RUC)

The repeating unit cell (RUC) is the smallest element in the periodic material which by repeating this element in all directions, the same structure of the material will be obtained. RUC's can be used for honeycombs that are periodic and without any defects. Three shapes of honeycombs were studied: square honeycombs, equilateral triangular honeycombs and regular hexagonal honeycombs. The RUC for all the shapes are shown in figure (3.3). The unit cell for the hexagonal is the same unit cell that had been used by Warren and Kraynik (1987) and also was used by Chen et al (1999). The equilateral triangular RUC that had been used in this study is the same as the RUC that had been used in Taylor et al (2011).



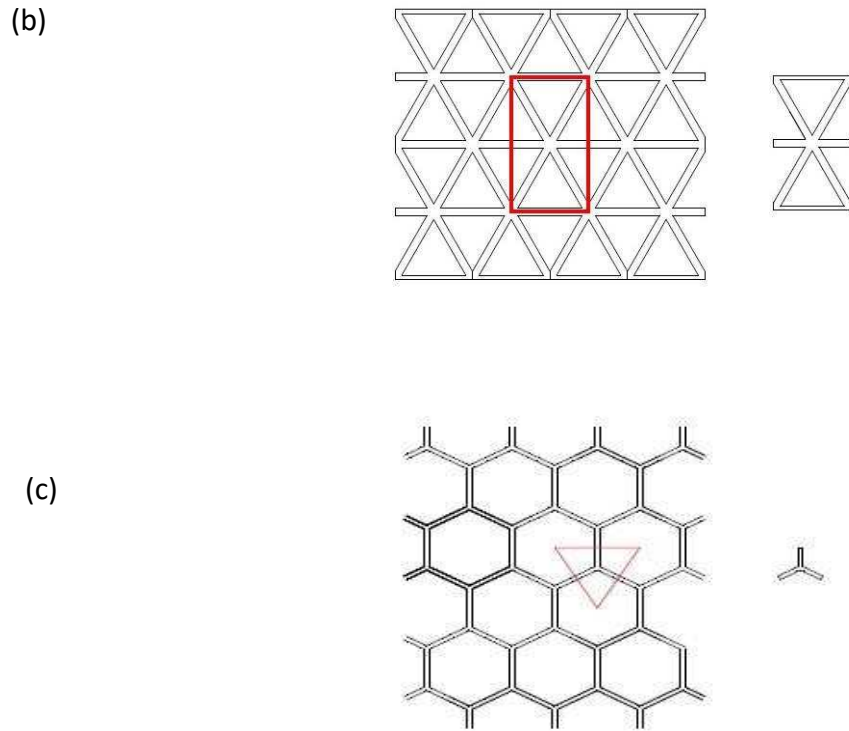


Figure 3.3: RUC for (a) Square (b) Equilateral triangle (c) Regular hexagon

### 3.3 Finite Element Method

The Finite Element Method (FEM) is a powerful tool to solve a different types of problems including solid mechanics, heat, electric, fluids and much more and has the ability to deal with complicated geometries. In this research, finite element approximations were used to solve for the coupled differential equations of elasticity, heat, electric, magnetic and moisture to find the effective properties of different shapes of two-dimensional honeycombs. The FEM has several major steps in order to get the final solution.

### 3.3.1 Discretization

The first step is discretization of the body into small elements that are connected by nodes and these nodes will have the degrees of freedom, a linear approximation can be performed to find any value for any point between the nodes. The type of the elements can vary depending on the problem and on the required accuracy of the approximation. Since this research is dealing with a two-dimensional problem in plane stress, a four-noded plane elasticity element has been chosen to discretize the unit cell of the honeycombs. Each node will have six degrees of freedom represented by displacement in the  $X_1$  direction ( $u$ ), displacement in the  $X_2$  direction ( $v$ ), electric potential ( $\phi$ ), magnetic potential ( $\Psi$ ), temperature change ( $\theta$ ) and moisture concentration change ( $m$ ). As it can be seen later in this chapter, a range of boundary conditions were used to find these degrees of freedom for the different shapes of unit cells and then finding the effective properties. A more accurate model can be achieved by making the elements smaller to have more nodes in the discretized body. But, this will make the problem more complicated and will need higher processing power. This constant trade-off between accuracy and computational expense is an issue for all finite element models.

### 3.3.2 Weak form

Finding the weak formulation is one of the most important steps in Finite Element that allowing to ease the requirement of continuity and make the differential equations much easier to deal with. Original equation is multiplied by an arbitrary function, integrated over the domain and set equal to zero.

$$\begin{aligned}
0 &= \int_A -\delta u \left\{ \frac{\partial}{\partial x} \left[ c_{11} \frac{\partial u}{\partial x} + c_{12} \frac{\partial v}{\partial y} + c_{16} \left( \frac{\partial u}{\partial y} + \frac{\partial v}{\partial x} \right) + e_{11} \frac{\partial \phi}{\partial x} + e_{21} \frac{\partial \phi}{\partial y} + d_{11} \frac{\partial \psi}{\partial x} + d_{21} \frac{\partial \psi}{\partial y} - \beta_{11} \theta - \zeta_{11} m \right] \right. \\
&+ \left. \frac{\partial}{\partial y} \left[ c_{16} \frac{\partial u}{\partial x} + c_{26} \frac{\partial v}{\partial y} + c_{66} \left( \frac{\partial u}{\partial y} + \frac{\partial v}{\partial x} \right) + e_{16} \frac{\partial \phi}{\partial x} + e_{26} \frac{\partial \phi}{\partial y} + d_{16} \frac{\partial \psi}{\partial x} + d_{26} \frac{\partial \psi}{\partial y} - \beta_{12} \theta - \zeta_{12} m \right] \right\} dx dy \\
0 &= \int_A \left[ c_{11} \frac{\partial \delta u}{\partial x} \frac{\partial u}{\partial x} + c_{12} \frac{\partial \delta u}{\partial x} \frac{\partial v}{\partial y} + c_{16} \frac{\partial \delta u}{\partial x} \left( \frac{\partial u}{\partial y} + \frac{\partial v}{\partial x} \right) + e_{11} \frac{\partial \delta u}{\partial x} \frac{\partial \phi}{\partial x} + e_{21} \frac{\partial \delta u}{\partial x} \frac{\partial \phi}{\partial y} + d_{11} \frac{\partial \delta u}{\partial x} \frac{\partial \psi}{\partial x} \right. \\
&+ d_{21} \frac{\partial \delta u}{\partial x} \frac{\partial \psi}{\partial y} - \beta_{11} \frac{\partial \delta u}{\partial x} \theta - \zeta_{11} \frac{\partial \delta u}{\partial x} m + c_{16} \frac{\partial \delta u}{\partial y} \frac{\partial u}{\partial x} + c_{26} \frac{\partial \delta u}{\partial y} \frac{\partial v}{\partial y} + c_{66} \frac{\partial \delta u}{\partial y} \left( \frac{\partial u}{\partial y} + \frac{\partial v}{\partial x} \right) + e_{16} \frac{\partial \delta u}{\partial y} \frac{\partial \phi}{\partial x} \\
&+ \left. e_{26} \frac{\partial \delta u}{\partial y} \frac{\partial \phi}{\partial y} + d_{16} \frac{\partial \delta u}{\partial y} \frac{\partial \psi}{\partial x} + d_{26} \frac{\partial \delta u}{\partial y} \frac{\partial \psi}{\partial y} - \beta_{12} \frac{\partial \delta u}{\partial y} \theta - \zeta_{12} \frac{\partial \delta u}{\partial y} m \right\} dx dy - \int_S \tau_x \delta u ds \quad (3.10)
\end{aligned}$$

$$\begin{aligned}
0 &= \int_A -\delta v \left\{ \frac{\partial}{\partial x} \left[ c_{16} \frac{\partial u}{\partial x} + c_{26} \frac{\partial v}{\partial y} + c_{66} \left( \frac{\partial u}{\partial y} + \frac{\partial v}{\partial x} \right) + e_{16} \frac{\partial \phi}{\partial x} + e_{26} \frac{\partial \phi}{\partial y} + d_{16} \frac{\partial \psi}{\partial x} + d_{26} \frac{\partial \psi}{\partial y} - \beta_{12} \theta - \zeta_{12} m \right] \right. \\
&+ \left. \frac{\partial}{\partial y} \left[ c_{12} \frac{\partial u}{\partial x} + c_{22} \frac{\partial v}{\partial y} + c_{26} \left( \frac{\partial u}{\partial y} + \frac{\partial v}{\partial x} \right) + e_{12} \frac{\partial \phi}{\partial x} + e_{22} \frac{\partial \phi}{\partial y} + d_{12} \frac{\partial \psi}{\partial x} + d_{22} \frac{\partial \psi}{\partial y} - \beta_{22} \theta - \zeta_{22} m \right] \right\} dx dy
\end{aligned}$$

$$\begin{aligned}
0 &= \int_A \left[ c_{16} \frac{\partial \delta v}{\partial x} \frac{\partial u}{\partial x} + c_{26} \frac{\partial \delta v}{\partial x} \frac{\partial v}{\partial y} + c_{66} \frac{\partial \delta v}{\partial x} \left( \frac{\partial u}{\partial y} + \frac{\partial v}{\partial x} \right) + e_{16} \frac{\partial \delta v}{\partial x} \frac{\partial \phi}{\partial x} + e_{26} \frac{\partial \delta v}{\partial x} \frac{\partial \phi}{\partial y} + d_{16} \frac{\partial \delta v}{\partial x} \frac{\partial \psi}{\partial x} \right. \\
&+ d_{26} \frac{\partial \delta v}{\partial x} \frac{\partial \psi}{\partial y} - \beta_{12} \frac{\partial \delta v}{\partial x} \theta - \zeta_{12} \frac{\partial \delta v}{\partial x} m + c_{12} \frac{\partial \delta v}{\partial y} \frac{\partial u}{\partial x} + c_{22} \frac{\partial \delta v}{\partial y} \frac{\partial v}{\partial y} + c_{26} \frac{\partial \delta v}{\partial y} \left( \frac{\partial u}{\partial y} + \frac{\partial v}{\partial x} \right) + e_{12} \frac{\partial \delta v}{\partial y} \frac{\partial \phi}{\partial x} \\
&+ \left. e_{22} \frac{\partial \delta v}{\partial y} \frac{\partial \phi}{\partial y} + d_{12} \frac{\partial \delta v}{\partial y} \frac{\partial \psi}{\partial x} + d_{22} \frac{\partial \delta v}{\partial y} \frac{\partial \psi}{\partial y} - \beta_{22} \frac{\partial \delta v}{\partial y} \theta - \zeta_{22} \frac{\partial \delta v}{\partial y} m \right\} dx dy - \int_S \tau_y \delta v ds \quad (3.11)
\end{aligned}$$

$$\begin{aligned}
0 &= \int_A -\delta \phi \left\{ \left[ e_{11} \frac{\partial u}{\partial x} + e_{12} \frac{\partial v}{\partial y} + e_{16} \left( \frac{\partial u}{\partial y} + \frac{\partial v}{\partial x} \right) - \varepsilon_{11} \frac{\partial \phi}{\partial x} - \varepsilon_{12} \frac{\partial \phi}{\partial y} - g_{11} \frac{\partial \psi}{\partial x} - g_{12} \frac{\partial \psi}{\partial y} + \gamma_1 \theta + X_1 m \right], x \right. \\
&+ \left. \left[ e_{21} \frac{\partial u}{\partial x} + e_{22} \frac{\partial v}{\partial y} + e_{26} \left( \frac{\partial u}{\partial y} + \frac{\partial v}{\partial x} \right) - \varepsilon_{12} \frac{\partial \phi}{\partial x} - \varepsilon_{22} \frac{\partial \phi}{\partial y} - g_{12} \frac{\partial \psi}{\partial x} - g_{22} \frac{\partial \psi}{\partial y} + \gamma_2 \theta + X_2 m \right], y \right\} dx dy
\end{aligned}$$

$$\begin{aligned}
0 = & \int_A [e_{11} \frac{\partial \delta \phi}{\partial x} \frac{\partial u}{\partial x} + e_{12} \frac{\partial \delta \phi}{\partial x} \frac{\partial v}{\partial y} + e_{16} \frac{\partial \delta \phi}{\partial x} (\frac{\partial u}{\partial y} + \frac{\partial v}{\partial x}) - \varepsilon_{11} \frac{\partial \delta \phi}{\partial x} \frac{\partial \phi}{\partial x} - \varepsilon_{12} \frac{\partial \delta \phi}{\partial x} \frac{\partial \phi}{\partial y} - g_{11} \frac{\partial \delta \phi}{\partial x} \frac{\partial \psi}{\partial x} \\
& - g_{12} \frac{\partial \delta \phi}{\partial x} \frac{\partial \psi}{\partial y} + \gamma_1 \frac{\partial \delta \phi}{\partial x} \theta + X_1 \frac{\partial \delta \phi}{\partial x} m + e_{21} \frac{\partial \delta \phi}{\partial y} \frac{\partial u}{\partial x} + e_{22} \frac{\partial \delta \phi}{\partial y} \frac{\partial v}{\partial y} + e_{26} \frac{\partial \delta \phi}{\partial y} (\frac{\partial u}{\partial y} + \frac{\partial v}{\partial x}) - \varepsilon_{12} \frac{\partial \delta \phi}{\partial y} \frac{\partial \phi}{\partial x} \\
& - \varepsilon_{22} \frac{\partial \delta \phi}{\partial y} \frac{\partial \phi}{\partial y} - g_{12} \frac{\partial \delta \phi}{\partial y} \frac{\partial \psi}{\partial x} - g_{22} \frac{\partial \delta \phi}{\partial y} \frac{\partial \psi}{\partial y} + \gamma_2 \frac{\partial \delta \phi}{\partial y} \theta + X_2 \frac{\partial \delta \phi}{\partial y} m] dx dy \\
& - \int_S (D_1 n_1 + D_2 n_2) \delta \phi ds \tag{3.12}
\end{aligned}$$

$$\begin{aligned}
0 = & \int_A -\delta \psi \{ [d_{11} \frac{\partial u}{\partial x} + d_{12} \frac{\partial v}{\partial y} + d_{16} (\frac{\partial u}{\partial y} + \frac{\partial v}{\partial x}) - g_{11} \frac{\partial \phi}{\partial x} - g_{12} \frac{\partial \phi}{\partial y} - \mu_{11} \frac{\partial \psi}{\partial x} - \mu_{12} \frac{\partial \psi}{\partial y} + \tau_1 \theta + \nu_1 m], x \\
& + [d_{21} \frac{\partial u}{\partial x} + d_{22} \frac{\partial v}{\partial y} + d_{26} (\frac{\partial u}{\partial y} + \frac{\partial v}{\partial x}) - g_{12} \frac{\partial \phi}{\partial x} - g_{22} \frac{\partial \phi}{\partial y} - \mu_{12} \frac{\partial \psi}{\partial x} - \mu_{22} \frac{\partial \psi}{\partial y} + \tau_2 \theta + \nu_2 m], y \} dx dy \\
0 = & \int_A [d_{11} \frac{\partial \delta \psi}{\partial x} \frac{\partial u}{\partial x} + d_{12} \frac{\partial \delta \psi}{\partial x} \frac{\partial v}{\partial y} + d_{16} \frac{\partial \delta \psi}{\partial x} (\frac{\partial u}{\partial y} + \frac{\partial v}{\partial x}) - g_{11} \frac{\partial \delta \psi}{\partial x} \frac{\partial \phi}{\partial x} - g_{12} \frac{\partial \delta \psi}{\partial x} \frac{\partial \phi}{\partial y} - \mu_{11} \frac{\partial \delta \psi}{\partial x} \frac{\partial \psi}{\partial x} \\
& - \mu_{12} \frac{\partial \delta \psi}{\partial x} \frac{\partial \psi}{\partial y} + \tau_1 \frac{\partial \delta \psi}{\partial x} \theta + \nu_1 \frac{\partial \delta \psi}{\partial x} m + d_{21} \frac{\partial \delta \psi}{\partial y} \frac{\partial u}{\partial x} + d_{22} \frac{\partial \delta \psi}{\partial y} \frac{\partial v}{\partial y} + d_{26} \frac{\partial \delta \psi}{\partial y} (\frac{\partial u}{\partial y} + \frac{\partial v}{\partial x}) - g_{12} \frac{\partial \delta \psi}{\partial y} \frac{\partial \phi}{\partial x} \\
& - g_{22} \frac{\partial \delta \psi}{\partial y} \frac{\partial \phi}{\partial y} - \mu_{12} \frac{\partial \delta \psi}{\partial y} \frac{\partial \psi}{\partial x} - \mu_{22} \frac{\partial \delta \psi}{\partial y} \frac{\partial \psi}{\partial y} + \tau_2 \frac{\partial \delta \psi}{\partial y} \theta + \nu_2 \frac{\partial \delta \psi}{\partial y} m] dx dy \\
& - \int_S (D_1 n_1 + D_2 n_2) \delta \psi ds \tag{3.13}
\end{aligned}$$

$$0 = \int_A \delta \theta \left[ -\frac{\partial}{\partial x} (K_x^\theta \frac{\partial \theta}{\partial x}) - \frac{\partial}{\partial y} (K_y^\theta \frac{\partial \theta}{\partial y}) \right] dx dy$$

$$0 = \int_A (K_x^\theta \frac{\partial \delta \theta}{\partial x} \frac{\partial \theta}{\partial x}) + (K_y^\theta \frac{\partial \delta \theta}{\partial y} \frac{\partial \theta}{\partial y}) dx dy - \int_S q_n^\theta \delta \theta ds \tag{3.14}$$

$$0 = \int_A \delta m \left[ -\frac{\partial}{\partial x} \left( K_x^m \frac{\partial m}{\partial x} \right) - \frac{\partial}{\partial y} \left( K_y^m \frac{\partial m}{\partial y} \right) \right] dx dy$$

$$0 = \int_A \left( K_x^m \frac{\partial \delta m}{\partial x} \frac{\partial m}{\partial x} \right) + \left( K_y^m \frac{\partial \delta m}{\partial y} \frac{\partial m}{\partial y} \right) dx dy - \int_S q_n^m \delta m ds \quad (3.15)$$

The FE approximation can be seen bellow:

$$u(x, y) = \sum_{j=1}^n u_j N_j^u(x, y) \quad (3.16)$$

$$\partial u = N_j^u \quad (3.17)$$

$$v(x, y) = \sum_{j=1}^n v_j N_j^v(x, y) \quad (3.18)$$

$$\partial v = N_j^v \quad (3.19)$$

$$\phi(x, y) = \sum_{j=1}^n \phi_j N_j^\phi(x, y) \quad (3.20)$$

$$\partial \phi = N_j^\phi \quad (3.21)$$

$$\psi(x, y) = \sum_{j=1}^n \psi_j N_j^\psi(x, y) \quad (3.22)$$

$$\partial \psi = N_j^\psi \quad (3.23)$$

$$\theta(x, y) = \sum_{j=1}^n \theta_j N_j^\theta(x, y) \quad (3.24)$$

$$\partial \theta = N_j^\theta \quad (3.25)$$

$$m(x, y) = \sum_{j=1}^n m_j N_j^m(x, y) \quad (3.26)$$

$$\partial m = N_j^m \quad (3.27)$$

### 3.3.3 Element matrices

The element matrices can be shown as follow:

$$\begin{bmatrix} [K^{11}] & [K^{12}] & [K^{13}] & [K^{14}] & [K^{15}] & [K^{16}] \\ [K^{21}] & [K^{22}] & [K^{23}] & [K^{24}] & [K^{25}] & [K^{26}] \\ [K^{31}] & [K^{32}] & [K^{33}] & [K^{34}] & [K^{35}] & [K^{36}] \\ [K^{41}] & [K^{42}] & [K^{43}] & [K^{44}] & [K^{45}] & [K^{46}] \\ [0] & [0] & [0] & [0] & [K^{55}] & [0] \\ [0] & [0] & [0] & [0] & [0] & [K^{66}] \end{bmatrix} \begin{Bmatrix} \{u\} \\ \{v\} \\ \{\phi\} \\ \{\psi\} \\ \{\theta\} \\ \{m\} \end{Bmatrix} = \begin{Bmatrix} \{F^1\} \\ \{F^2\} \\ \{F^3\} \\ \{F^4\} \\ \{F^5\} \\ \{F^6\} \end{Bmatrix} \quad (3.28)$$

After finding the element matrices, the only thing that is left to solve for the unknowns is the assembly in the global matrix and applying the boundary conditions. The elements of the matrix equations for the Ritz model are provided in the Appendix.

## 3.4 Boundary conditions and the effective properties

Specific boundary conditions must be imposed to find the solution for every loading case and to find the effective property that is associated with that boundary condition. This section will contain the boundary conditions based on the effective property that is required. The boundary conditions that have been used will be explained for every case.

### 3.4.1 Effective elastic properties

An overview of effective elastic properties for pure elastic foams has been given in an earlier chapter, but the highlights are given here. For the square unit cell and the equilateral

triangle unit cell, a prescribed boundary conditions were applied to find the forces and the displacement in the unit cell and then are analyzed find the effective elastic properties. The procedure from Li et al. (2004) is used in this study to obtain the effective elastic properties. To find the effective modulus of elasticity ( $E_1$ ) and Poisson's ratio ( $\nu_{12}$ ) for the square and the triangular unit cells, an arbitrary displacement was applied in the  $X_1$  direction at the right boundary of the unit cell, constraints at bottom and left boundaries were provided. The magnitude is irrelevant since the response is linear. After doing the finite element analysis and finding all the forces and displacements in the unit cell,  $E_1$  and  $\nu_{12}$  can be found easily by simple mechanics using the following equations :

$$E_1 = \frac{-F_1}{L_2 * h * \varepsilon_1} \quad (3.29)$$

$$\nu_{12} = \frac{-u_2}{\varepsilon_1 * L_2} \quad (3.30)$$

where:  $F_1$  is the total force in the  $X_1$  direction,  $h$  is the thickness of the cell in the out of plane direction and can be taken as 1,  $\varepsilon_1$  is the strain in the  $X_1$  direction and  $L_2$  is the cell length in  $X_2$  direction.  $E_2$  and  $\nu_{21}$  can be found using the same method but applying the displacement in the  $X_2$  direction instead and find them using :

$$E_2 = \frac{-F_2}{L_1 * h * \varepsilon_2} \quad (3.31)$$

$$\nu_{21} = \frac{-u_1}{\varepsilon_2 * L_1} \quad (3.32)$$

To find the shear modulus  $G_{12}$ , a biaxial displacement is applied. A tensile displacement is imposed in the  $X_1$  direction and a compressive displacement is imposed in the  $X_2$  is applied.

The elastic constant  $G_{12}$  can then be found by:

$$G_{12} = \frac{F_1/L_2 - F_2/L_1}{2h(\varepsilon_1 - \varepsilon_2)} \quad (3.33)$$

After finding all the effective properties, the constitutive relation that relates the strains to the stresses by the compliance tensors  $S_{ijkl}$  where:

$$\varepsilon_{ij} = S_{ijkl} \sigma_{kl} \quad (3.34)$$

$$S_{1111} = \frac{1}{E_1} \quad (3.35)$$

$$S_{1111} = \frac{1}{E_1} \quad (3.36)$$

$$S_{1122} = -\frac{\nu_{21}}{E_1} \quad (3.37)$$

$$S_{2211} = -\frac{\nu_{12}}{E_1} \quad (3.38)$$

$$S_{2222} = \frac{1}{E_1} \quad (3.39)$$

$$S_{3333} = \frac{1}{G_{12}} \quad (3.40)$$

The same way, the stresses can be related to the strains by the stiffnesses tensors  $C_{ijkl}$  :

$$\sigma_{ij} = C_{ijkl} \varepsilon_{kl} \quad (3.41)$$

$$C_{1111} = \frac{E_1}{(1-\nu_{12}\nu_{21})} \quad (3.42)$$

$$C_{1122} = \frac{\nu_{21}E_1}{(1-\nu_{12}\nu_{21})} \quad (3.43)$$

$$C_{2211} = \frac{\nu_{12}E_2}{(1-\nu_{12}\nu_{21})} \quad (3.44)$$

$$C_{2222} = \frac{E_2}{(1-\nu_{12}\nu_{21})} \quad (3.45)$$

$$C_{3333} = G_{12} \quad (3.46)$$

Reduced stiffnesses were obtained since this research is dealing with plane stresses only. The relation between the compliances and the stiffnesses can be computed using:

$$[S] = [C]^{-1} \quad (3.47)$$

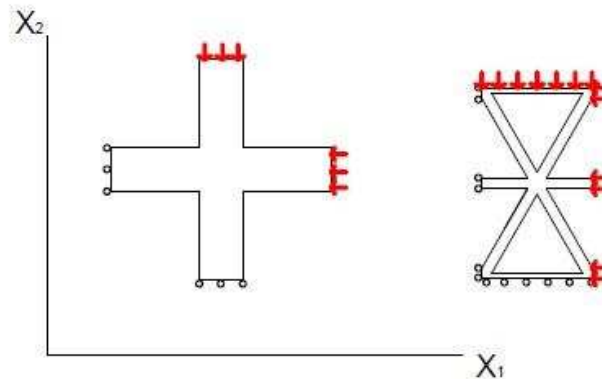


Figure 3.4: The boundary conditions used to find the effective properties of the square and the triangular unit cells.

For the hexagonal honeycombs, because a displacement in only one direction cannot be applied due to the inclined boundaries, the procedure was a bit different. Affine motion, as used by Heyliger and McMeeking (2001), was applied to the boundary nodes using the same procedure that been used in Chen et al.(1999) and also by Steadman et al. (2014). An arbitrary strain in the  $X_1$  direction was imposed and the average stress was found. The same strain value in the  $X_2$  direction was applied and the average stress was found. The applied nodal displacements were applied as:

$$u_i = S_{ij}x_j \quad (3.48)$$

Where:  $u_i$  are the nodal displacements,  $S_{ij}$  are the components of strain and  $x_j$  are the nodal coordinates.

The average stress can be calculated by using:

$$\sigma_{jk} = \frac{\sum_{i=1}^N F_j^i x_k}{V} \quad (3.49)$$

Here:  $\sigma_{jk}$  is the average stress,  $F_j^i$  is the reaction force in the j-th direction at the i-th node, N is the number of boundary nodes,  $x_k$  is the nodal coordinate and V is the volume and in this case is equal to the area of the unit cell. Then, the effective elastic properties can be found by using equations 3.34 to 3.47 as before.

### 3.4.2 The effective electric and magnetic properties

Very few studies have been published on cellular solids that are made from piezoelectric/ piezomagnetic materials and non of them explained or pointed out the boundary conditions that have been used. For that reason, a set of boundary conditions that is logically consistent with those used for the recovery of effective elastic constants were used to find the effective piezoelectric and piezomagnetic coefficients for the honeycombs of the present study. To find the piezoelectric coefficient of, for example,  $e_{11}$ , an electric potential was applied on the right boundary nodes and a different value on the left boundary nodes with linear increase for the boundary nodes between them. Constraints were provided for all the boundaries except the right side and the unit cell was free to move in the  $X_1$  direction. Calculating the strain that is caused by applying the electric field in the  $X_1$  direction will help in finding  $e_{11}$  by using the following equations:

$$S_{ij} = E_K l_{kij} \quad (3.50)$$

And

$$e_{kij} = c_{jklm} l_{ilm} \quad (3.51)$$

Here:  $S_{ij}$  is the strain components,  $E_K$  is the electric field components,  $l_{kij}$  are the components of the piezoelectric tensor (strain coefficients) and  $c_{jklm}$  are the components of the elastic stiffnesses that are calculated from the previous steps. To find  $e_{21}$ , the same procedure was followed except making the unit cell free to move in the  $X_2$  direction instead of  $X_1$  direction. For the piezomagnetic coefficients  $d_{kij}$ , the same approach was used, since both have the same differential equation, but by applying magnetic potential instead and using the following equations:

$$S_{ij} = B_K q_{kij} \quad (3.52)$$

And

$$d_{kij} = C_{jklm} q_{ilm} \quad (3.53)$$

This approach is very similar to the method used to recover the effective  $C_{ij}$ .

### 3.4.3 The effective thermal expansion and moisture expansion coefficients

To find the effective thermal expansion coefficient, a temperature difference of (+100K) was applied on all the external boundary nodes of the unit cell with constraints imposed on the left and bottom boundaries. The increase in the area will be calculated since this research is dealing with two-dimensional unit cell. The thermal expansion coefficient for the area can be calculated using:

$$\alpha = \frac{\Delta A}{2A \cdot \Delta \theta} \quad (3.54)$$

where  $\Delta A$  is the change in the area due to the change in temperature,  $A$  is the original area and  $\Delta \theta$  is the change in the temperature.

For the moisture expansion coefficient, the same procedure can be used since they both have the same differential equation. This property was not considered in this work.

### 3.4.4 The effective pyroelectric and pyromagnetic coefficients

The change in the temperature will cause the honeycomb to deform and have consistent strains. These strains, for the MEE material, in return will generate electric and magnetic potentials. The calculation of the pyroelectric coefficients is a relatively simple process and is accomplished by multiplying the piezoelectric coefficients by the thermal expansion coefficient. The pyromagnetic coefficients can also simply calculated by multiplying piezomagnetic coefficients by the thermal expansion coefficient.

### 3.5 The Relative Density

The relative density of the foam and honeycombs is an important property and all the mechanical properties of the cellular solid have been attached to the relative density (Equation 2.1). The relative density for honeycombs depends on the (t/l) ratio and can be found for every unit cell shape according to the following equation as found in Gibson and Ashby (1997):

$$\text{For squares:} \quad \frac{\rho^*}{\rho_s} = 2 \frac{t}{l} \left(1 - \frac{1}{2} \frac{t}{l}\right) \quad (3.55)$$

$$\text{For equilateral triangles:} \quad \frac{\rho^*}{\rho_s} = 2\sqrt{3} \frac{t}{l} \left(1 - \frac{\sqrt{3}}{2} \frac{t}{l}\right) \quad (3.56)$$

$$\text{For regular hexagons:} \quad \frac{\rho^*}{\rho_s} = \frac{2}{\sqrt{3}} \frac{t}{l} \quad (3.57)$$

### 3.6 Computational Model

A finite element program was written using MATLAB to solve for the unknown variables. The code will read the input file which contains the number of the elements, number of nodes, material properties, coordinates of the nodes, connectivity array and the numbers and values of the essential and the natural boundary conditions. After reading the input file, the code constructs the elements matrices and assemble them immediately in the global matrix in a way that half-band width can be obtain. In other words, the code will find every variable in each node before jumping to the next one and that will reduce the time of processing significantly. Finally, the code will find the values for the wanted variables based on the given boundary conditions. This code is capable in dealing with elasticity, electric, magnetic, thermal and moisture problems individually or combined together. A copy of the code can be found in the Appendix.

## CHAPTER 4: RESULTS AND DISCUSSION

This chapter presents the results obtained according to the method explained extensively in the previous chapter. Some of the results will be compared with the results of existing studies and some of the new behaviors will be discussed and explained. All the results of this chapter are obtained for three different unit cells (square, equilateral triangles and regular hexagons) with ratios of (t/l) ranging from (0.02) to (0.1) with an increment of (0.02) that will give a different basic effective properties as a function of the relative densities. The analysis is based on plane stress.

### 4.1 The relative density:

The results of the relative densities were giving according to equations 3.33, 3.34 and 3.35 from Chapter 3. These can be found in Table 2.

Table 2. The relative density ( $\frac{\rho^*}{\rho_s}$ ) for the square, equilateral triangle and the regular hexagon unit cells.

t/l	$\frac{\rho^*}{\rho_s}$		
	Square	Equilateral Triangle	Regular Hexagon
0.02	0.0396	0.068082	0.023094
0.04	0.0784	0.133764	0.046188
0.06	0.1164	0.197046	0.069282
0.08	0.1536	0.257928	0.092376
0.1	0.19	0.31641	0.11547

For the same  $(t/l)$  ratio, the equilateral triangle cellular solids shows the highest relative density and the hexagonal cellular solids has the lowest relative density compared to the other cell shapes.

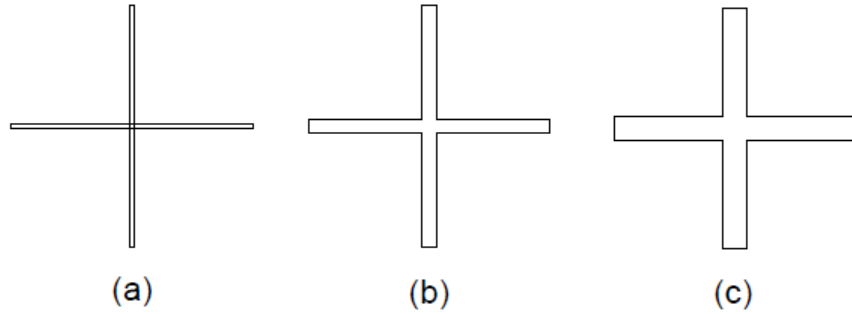


Figure 4.1: Different  $(t/l)$  ratios for the square unit cell (a)  $t/l = 0.02$  (b)  $t/l = 0.06$  (c)  $t/l = 0.1$

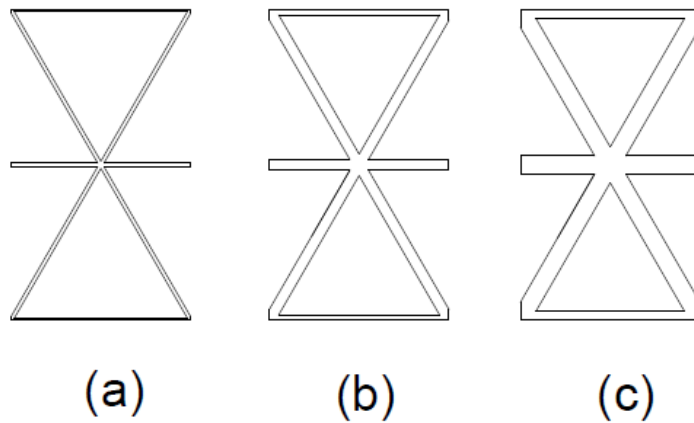


Figure 4.2: Different  $(t/l)$  ratios for the equilateral triangle unit cell (a)  $t/l = 0.02$  (b)  $t/l = 0.06$  (c)  $t/l = 0.1$

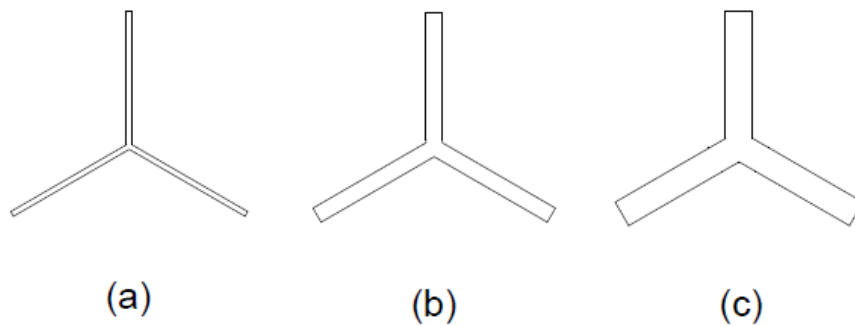


Figure 4.3: Different  $(t/l)$  ratios for the regular hexagon unit cell (a)  $t/l = 0.02$  (b)  $t/l = 0.06$  (c)  $t/l = 0.1$

## 4.2 The elastic properties:

Finding the elastic properties as quantified by the components of the stiffness and compliance tensors is an essential task prior to calculating both the piezoelectric and the piezomagnetic properties. Also, finding the effective properties, especially the effective modulus of elasticity, is very important to validate the computational procedure that has been followed in this study by comparing the obtained elastic properties to the existing studies that are done by other researchers.

For the square unit cell, the elastic properties, the stiffness tensors and the compliance tensors are shown in Table 3, 4 and 5. The ratio  $\left(\frac{E}{E_m}\right)$  was obtained so that the results can be compared to only work that has been found on square honeycombs by Gulati (1975). Gulati's found a linear relationship between  $\left(\frac{E}{E_m}\right)$  and  $(t/l)$  as follows:

$$\frac{E_1}{E_{m1}} = \frac{E_2}{E_{m2}} = \frac{t}{l} \quad 4.1$$

The comparison of the results can be seen in Figure 4.4 and the results showed a very good agreement with the results of Gulati (1975) who used one-dimensional elements, with the present results giving slightly larger magnitudes. The linear behavior of every elastic property, which can be seen clearly in each of the Figures, for the square honeycombs is explained by that the square unit cells are only experiencing tension or compression deformations in their cell walls and there is no bending in the cell walls during the deformations imposed as part of this analysis. Figures 4.5 and 4.6 shows the  $E_1$  and the  $G_{12}$  moduli respectively

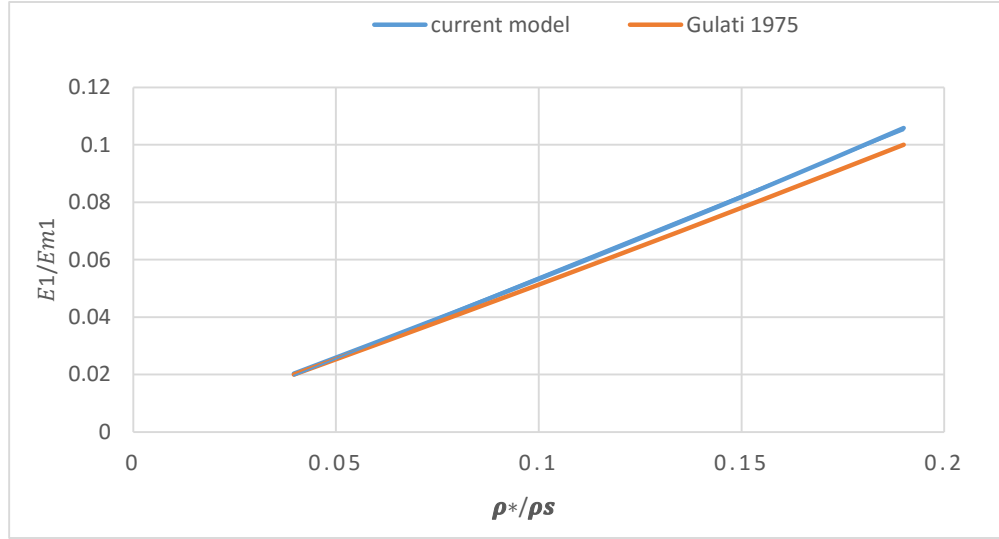


Figure 4.4: Comparison of results with Gulati (1975) for the square honeycombs

Table 3. Elastic properties for the square honeycomb. E and G in ( $10^9$  N/m<sup>2</sup>),  $\nu$  is dimensionless.

t/l	$E_1$	$E_2$	$\nu_{12}$	$\nu_{21}$	$G_{12}$	$E_1/Em_1$	$E_2/Em_2$
0.02	3.1288	3.1288	0.021	0.021	1.5322	0.02034	0.020337
0.04	6.35	6.35	0.037	0.037	3.1	0.04127	0.04127
0.06	9.621	9.621	0.052	0.052	4.6	0.06253	0.062537
0.08	12.91	12.91	0.065	0.065	6.0682	0.08391	0.083915
0.1	16.28	16.28	0.079	0.079	7.54	0.10582	0.10582

Table 4. Compliance tensors for the square honeycomb in ( $10^{-9}$  m<sup>2</sup>/N)

t/l	$s_{11}$	$s_{12}$	$s_{21}$	$s_{22}$
0.02	0.31961135	0.0067118	0.3196114	0.652656
0.04	0.15748031	0.0058268	0.1574803	0.322581
0.06	0.1039393	0.0054048	0.1039393	0.217391
0.08	0.07745933	0.0050349	0.0774593	0.164794
0.1	0.06142506	0.0048526	0.0614251	0.132626

Table5. Stiffnesses tensors for the square honeycomb in ( $10^9 \text{ N/m}^2$ )

$t/l$	$c_{11}$	$c_{12}$	$c_{21}$	$c_{22}$	$c_{66}$
0.02	3.13018041	0.06573379	0.06573379	3.13018041	1.5322
0.04	6.35870507	0.23527209	0.23527209	6.35870507	3.1
0.06	9.64708572	0.50164846	0.50164846	9.64708572	4.6
0.08	12.9647762	0.84271045	0.84271045	12.9647762	6.0682
0.1	16.3822416	1.29419708	1.29419708	16.3822416	7.54

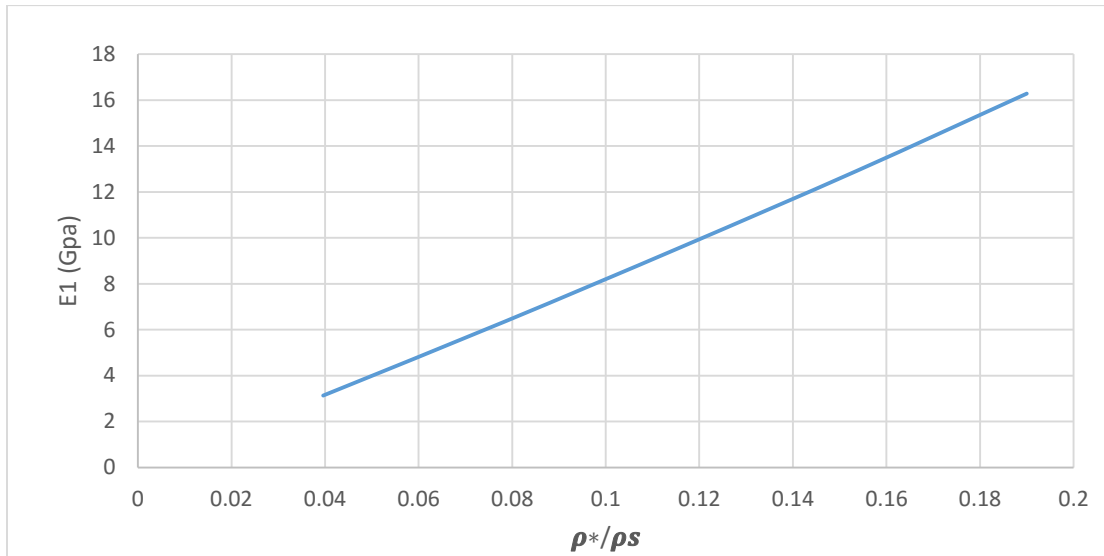


Figure 4.5: Modulus of elasticity  $E_1$  for the square honeycomb

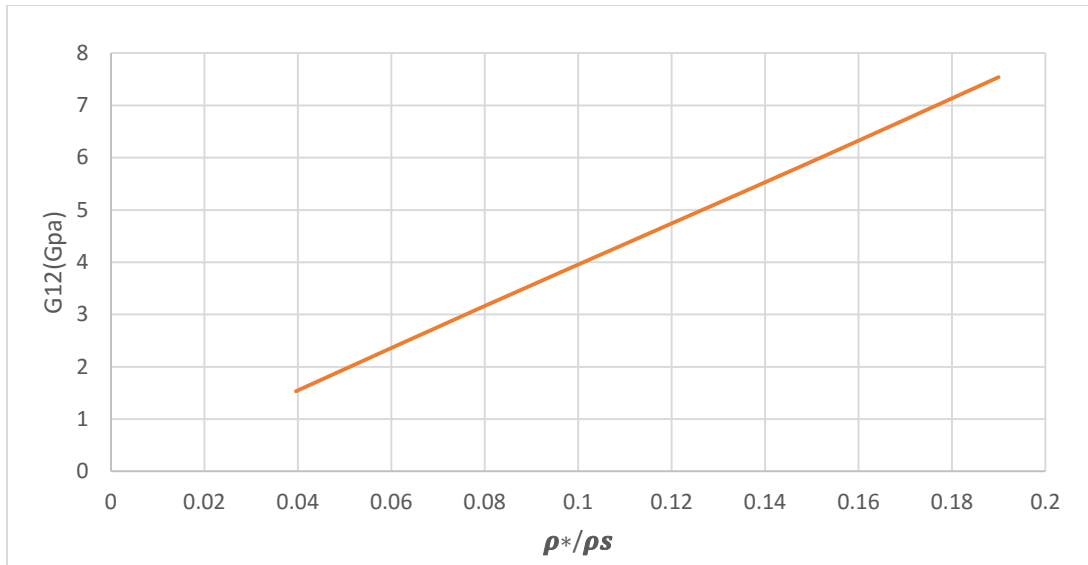


Figure 4.6: The shear modulus  $G_{12}$  for the square honeycomb

For the triangular honeycombs, the same linear behavior was observed of the modulus of elasticity and other elastic properties. Along with the linear increase with the increase of relative density, the triangular honeycombs are stiffer than the square honey combs because the behavior of the triangular honeycombs is similar to the behavior of trusses. The modulus of elasticity results for the triangular honeycomb were compared to the equation given by Hunt (1993), expressed by:

$$\frac{E_1}{E_{m1}} = \frac{E_2}{E_{m2}} = 1.15 \frac{t}{l} \quad 4.2$$

The results were also compared to equation 2.3 by Christensen (2000) which can be expressed in terms of the relative density by the relation:

$$\frac{E}{E_m} = \frac{1}{3} \left( \frac{\rho^*}{\rho_s} \right) \quad 4.3$$

Figure 4.7 shows the comparison between the present results and those of the previous two equations. The elastic properties and components of the stiffness and compliances tensors for the equilateral triangles are shown in tables 6, 7 and 8.

Table 6. The elastic properties for the equilateral triangular honeycomb

$t/l$	$E_1$	$E_2$	$\nu_{12}$	$\nu_{21}$
0.02	4.25	4.25	0.4	0.4
0.04	8.03	8.03	0.4278	0.4278
0.06	12.1	12.1	0.4457	0.4457
0.08	16.2	16.8	0.458	0.458
0.1	20.3	20.44	0.4642	0.4642

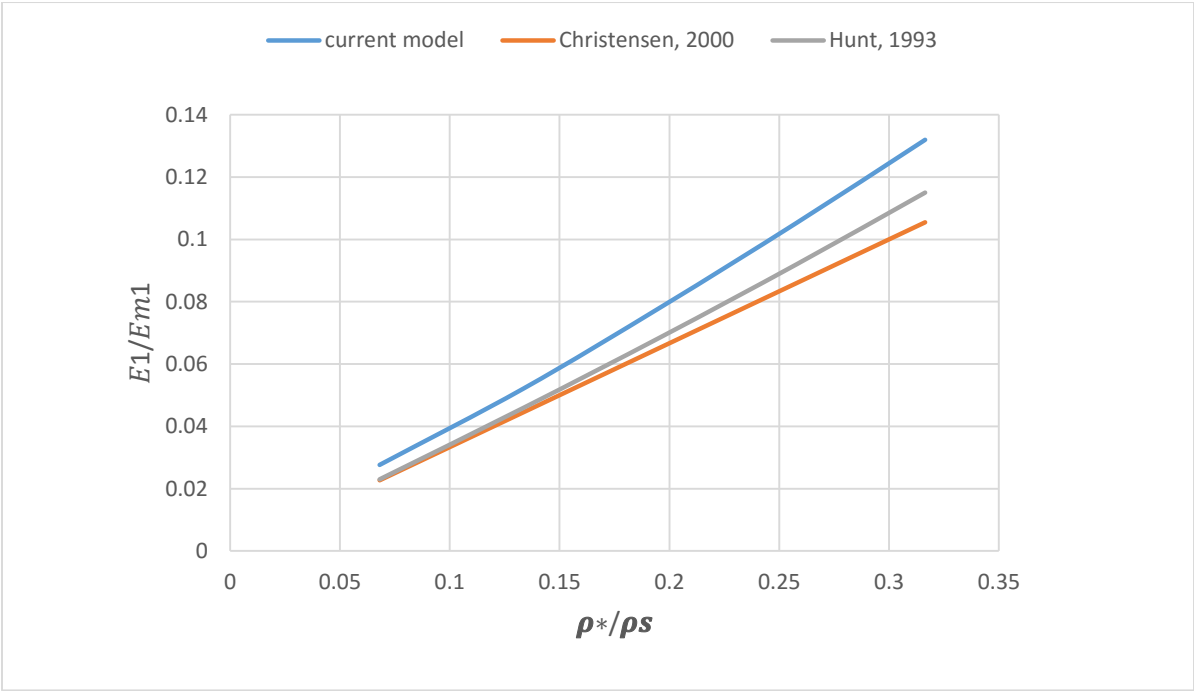


Figure 4.7. Comparison of results with existing studies for the triangular honeycomb

Table 7. Compliances tensors for the triangular honeycomb in ( $10^{-9} m^2/N$ )

t/l	$s_{11}$	$s_{12}$	$s_{21}$	$s_{22}$
0.02	0.23529412	0.09411765	0.09411765	0.23529412
0.04	0.124533	0.05327522	0.05327522	0.124533
0.06	0.08264463	0.03683471	0.03683471	0.08264463
0.08	0.0617284	0.0272619	0.0282716	0.05952381
0.1	0.04926108	0.02271037	0.022867	0.04892368

Table 8. Stiffnesses tensors for the triangular honeycomb in ( $10^9 N/m^2$ )

t/l	$c_{11}$	$c_{12}$	$c_{21}$	$c_{22}$
0.02	5.059524	2.02381	2.02381	5.059524
0.04	9.828796	4.204759	4.204759	9.828796
0.06	15.09949	6.729843	6.729843	15.09949
0.08	20.50021	9.389094	9.736838	21.25947
0.1	25.87575	12.01152	12.09436	26.0542

For the regular hexagonal honeycomb, the relationship between the elastic modulus and the relative density or the ratio (t/l) was not linear. This is primarily because of the bending deformations that are experienced in the cell walls even when only compression or tension loads were applied. That also is the reason why the hexagonal is the most flexible among the three cell shapes considered in this research since loads that are directly axially are typically the stiffest. The work on hexagons is enormous but this research will compare the results with only two studies. The first is the result of work by Gibson and Ashby (1997) and is expressed by the equation below:

$$\frac{E_1}{E_{m1}} = \frac{E_2}{E_{m2}} = \frac{4}{\sqrt{3}} \left(\frac{t}{l}\right)^3 \quad 4.4$$

The results are also compared with the equation of Steadman et al (2014):

$$\frac{E_1}{E_{m1}} = \frac{E_2}{E_{m2}} = 1.4135 \left(\frac{\rho^*}{\rho_s}\right)^{2.9837} \quad 4.5$$

Figure 4.8 shows the comparison between the obtained results and the two previous equations. Tables 9, 10 and 11 have the elastic properties, the compliances and the stiffnesses tensors. The present moduli were slightly higher than those obtained by others. The reason for this is that FEM for the equations of plane elasticity were used in this research unlike others who used simple mechanics or structural analysis approaches. For example, Steadman and co-workers (2014) have used the direct stiffness method along with planar frame analysis to get their results. The FEM method tends to give higher results for the elastic properties because it makes the solid stiffer for many of the deformation modes

Table 9. Elastic properties for the hexagonal honeycomb

$t/l$	$E_1$	$E_2$	$\nu_{12}$	$\nu_{21}$
0.02	0.003	0.003	1	1
0.04	0.032	0.032	0.9999	0.9999
0.06	0.088	0.088	0.9998	0.9998
0.08	0.22	0.22	0.9996	0.9996
0.1	0.368	0.368	0.9994	0.9994

Table 10. Compliances tensors for the square honeycomb in ( $10^{-9} m^2/N$ )

t/l	$s_{11}$	$s_{12}$	$s_{21}$	$s_{22}$
0.02	333.3333333	333.3	333.3	333.3333
0.04	31.25	31.24688	31.24688	31.25
0.06	11.36363636	11.35909	11.35909	11.36364
0.08	4.545454545	4.543636	4.543636	4.545455
0.1	2.717391304	2.715761	2.715761	2.717391

Table 11. Stiffnesses tensors for the hexagonal honeycomb in ( $10^9 N/m^2$ )

t/l	$c_{11}$	$c_{12}$	$c_{21}$	$c_{22}$
0.02	29.97003296	29.96704	29.97003	29.97003
0.04	160.0080004	159.992	159.992	160.008
0.06	219.9450357	219.8571	219.945	219.945
0.08	275.055011	274.945	274.945	275.055
0.1	306.7586943	306.5746	306.5746	306.7587

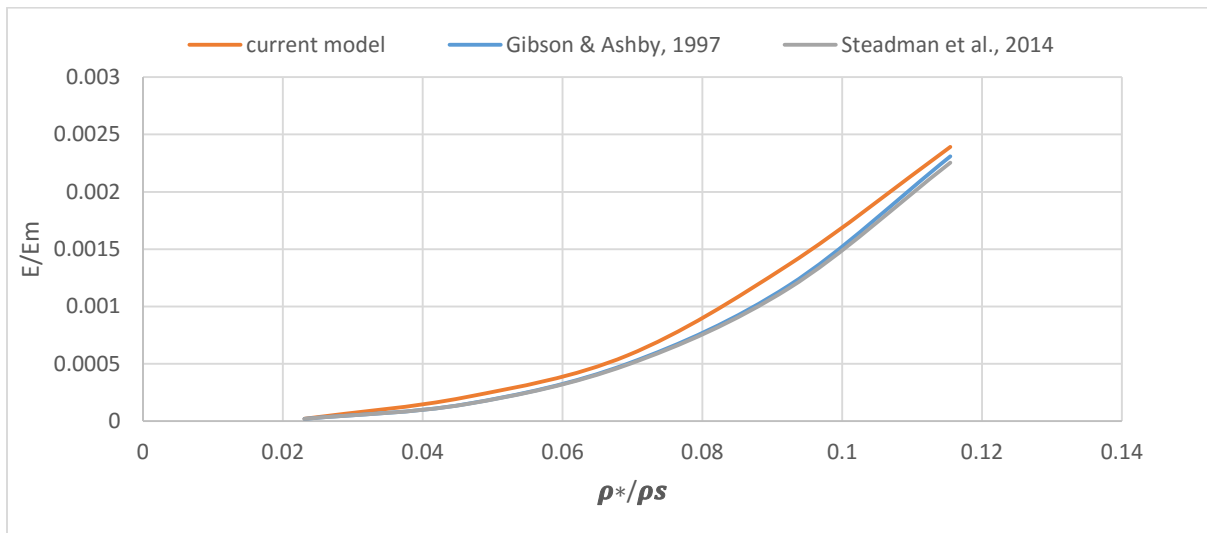


Figure 4.8: Comparison of results with existing studies for the hexagonal honeycomb

### 4.3 The effective piezoelectric properties:

The effective piezoelectric coefficients were also found for all of the unit cell shapes and all the (t/l) ratios. For the square honeycombs, the piezoelectric coefficients  $e_{11}$  and  $e_{22}$  showed a linear behavior when the relative density was increased while the piezoelectric coefficients  $e_{12}$  and  $e_{21}$  showed a polynomial increase when increasing the relative density. This behavior can be seen in Figures 4.9 and 4.10. The results of the piezoelectric coefficients provided in Table 12.

Table 12. Piezoelectric coefficients for the square honeycombs in (C/m<sup>2</sup>)

t/l	$e_{11}$	$e_{12}$	$e_{21}$	$e_{22}$
0.02	7.59069E-05	3.29E-09	3.29E-09	7.59069E-05
0.04	0.000154898	5.88E-08	5.88E-08	0.000154898
0.06	0.000235606	3.88E-07	3.88E-07	0.000235606
0.08	0.000316989	1.07E-06	1.07E-06	0.000316989
0.1	0.000409556	2.29E-06	2.29E-06	0.000409556

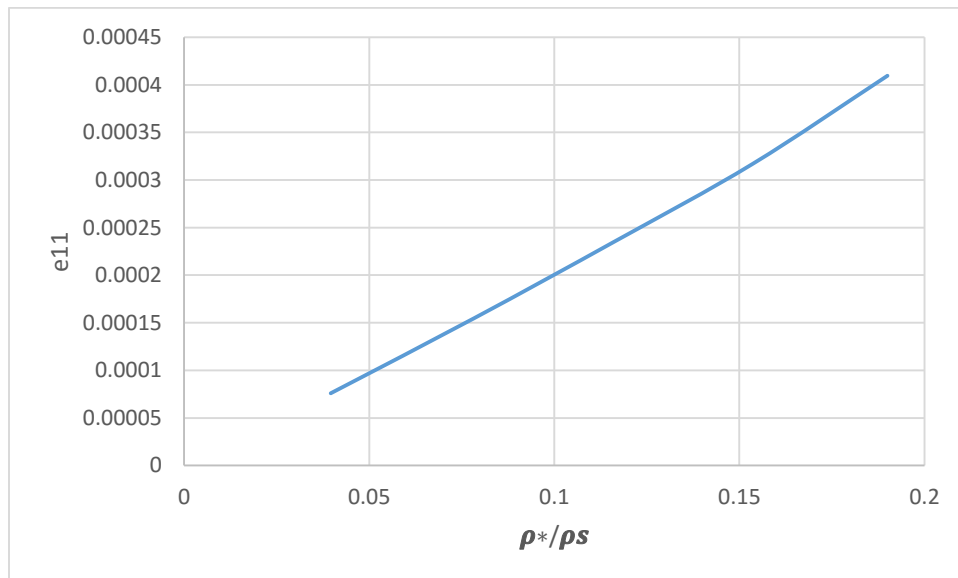


Figure 4.9: The  $e_{11}$  coefficient for the square honeycomb

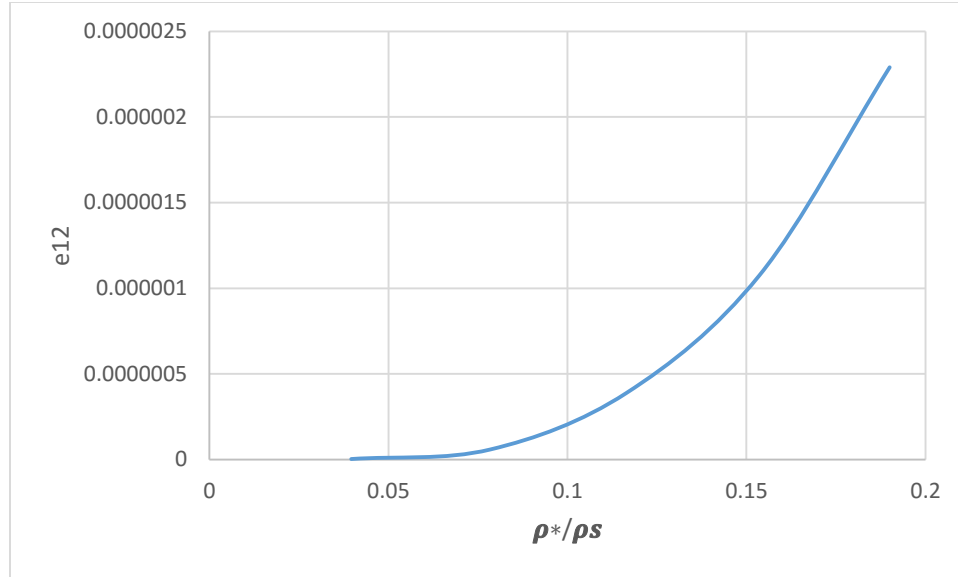


Figure 4.10: The  $e_{21}$  coefficient for the square honeycomb

For the equilateral triangular honeycombs, linear behavior also was obtained for the piezoelectric coefficients  $e_{11}$ ,  $e_{21}$  and  $e_{22}$ . The piezoelectric coefficients  $e_{12}$  showed a non-linear behavior with a negative value that means an increase in the dimension in the other direction where the electric potential was applied will occur. Table 13 and Figures 4.11 and 4.12 show the results of the equilateral triangular unit cells.

Table 13. Piezoelectric coefficients for the triangular honeycombs in ( $C/m^2$ ).

$t/l$	$e_{11}$	$e_{12}$	$e_{21}$	$e_{22}$
0.02	0.000311	-2.3E-05	-2.3E-05	0.000128
0.04	0.000601	-2.5E-05	-2.9E-05	0.000227
0.06	0.000916	-3.3E-05	-3.3E-05	0.000339
0.08	0.00123	-4.5E-05	-3.5E-05	0.00046
0.1	0.001547	-5.7E-05	-3.9E-05	0.000579

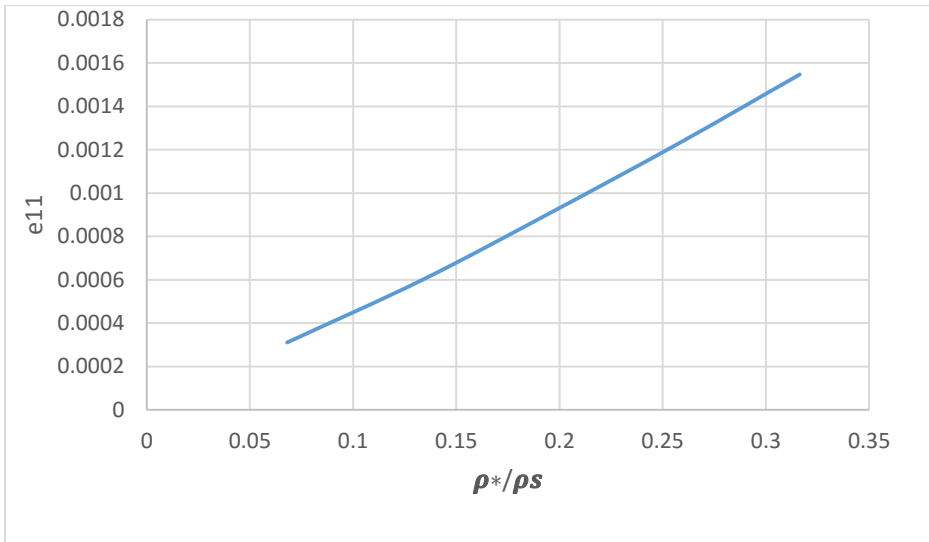


Figure 4.11: The  $e_{11}$  coefficient for the triangular honeycomb

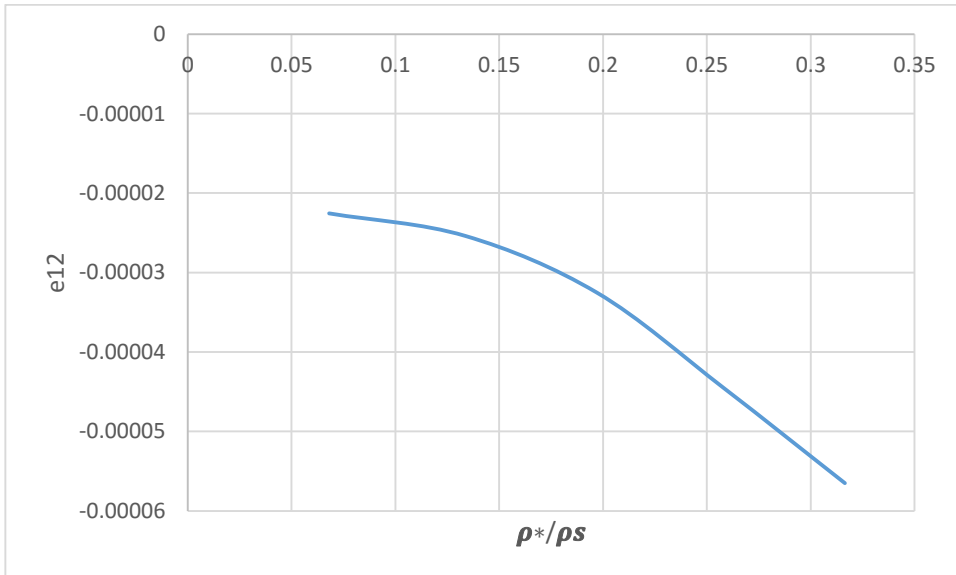


Figure 4.12. The  $e_{12}$  coefficient for the triangular honeycomb

For the regular hexagons, a non-linear increase in all the piezoelectric coefficients  $e_{11}$ ,  $e_{12}$ ,  $e_{21}$  and  $e_{22}$ . was noticed when the relative density was increased. The results for the regular hexagons is shown in Table 14, Figure 4.13 and Figure 4.14.

Table 14. Piezoelectric coefficients for the hexagonal honeycomb in (C/m<sup>2</sup>)

$t/l$	$e_{11}$	$e_{12}$	$e_{21}$	$e_{22}$
0.02	0.001187	-0.00092	0.001087	0.001664
0.04	0.006296	-0.00471	0.005796	0.008586
0.06	0.008579	-0.00615	0.00791	0.011382
0.08	0.010617	-0.00726	0.009799	0.013688
0.1	0.011689	-0.00768	0.010796	0.014728

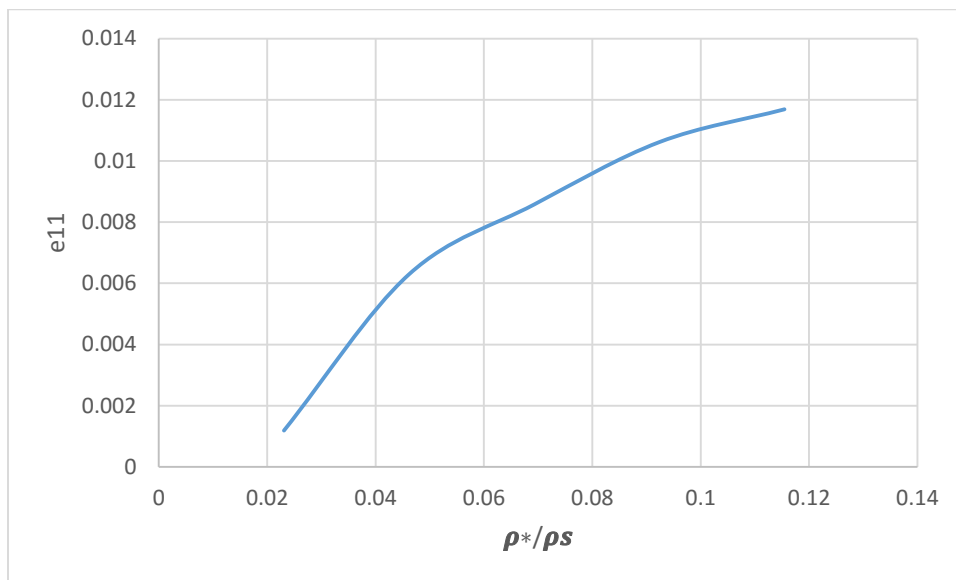


Figure 4.13. The  $e_{11}$  coefficient for the hexagonal honeycomb

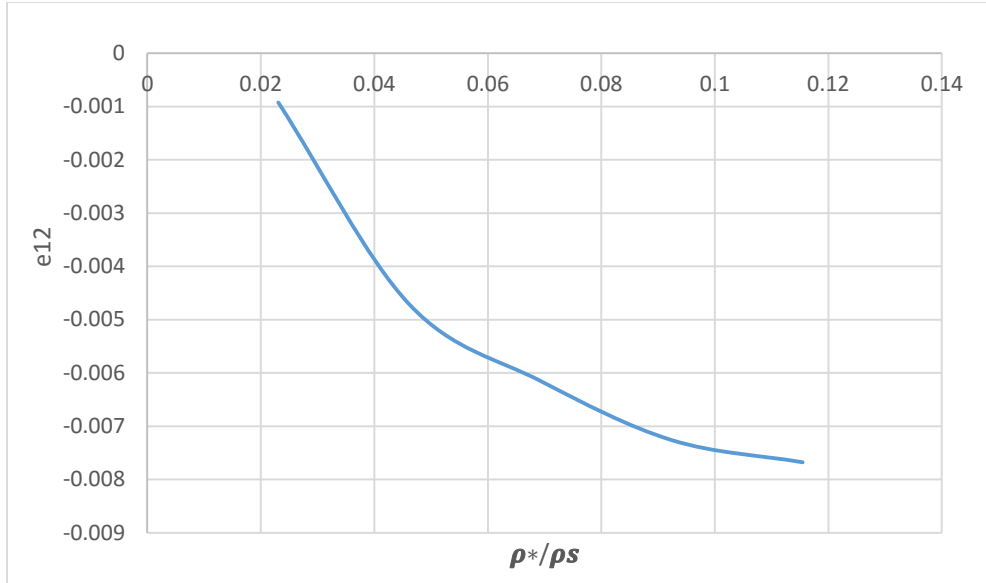


Figure 4.14. The  $e_{12}$  coefficient for the hexagonal honeycomb

#### 4.4 The effective piezomagnetic properties:

The effective piezomagnetic coefficients were found for varying (t/l) ratios and for all honeycomb shapes. The results were similar to those of the piezoelectric coefficients in how they changed with the increase of the relative density because they both have the same differential equations. For the square unit cell, the effective piezomagnetic coefficients  $d_{11}$  and  $d_{22}$  increased linearly while  $d_{12}$  and  $d_{21}$  increased non-linearly with the increase of the relative density. Table 15 shows the results for the square unit cell and figure 4.15 and 4.16 shows the behavior of the coefficients  $d_{11}$  and  $d_{21}$ .

Table 15. Piezomagnetic coefficients for the square honeycombs in (N/Am)

$t/l$	$d_{11}$	$d_{12}$	$d_{21}$	$d_{22}$
0.02	1.79E-03	7.73E-06	7.73E-06	0.001789
0.04	0.003642584	2.05E-05	2.05E-05	0.003643
0.06	0.005527684	4.29E-05	4.29E-05	0.005528
0.08	0.007422334	7.63E-05	7.63E-05	0.007422
0.1	0.009361632	0.00012	0.00012	0.009362

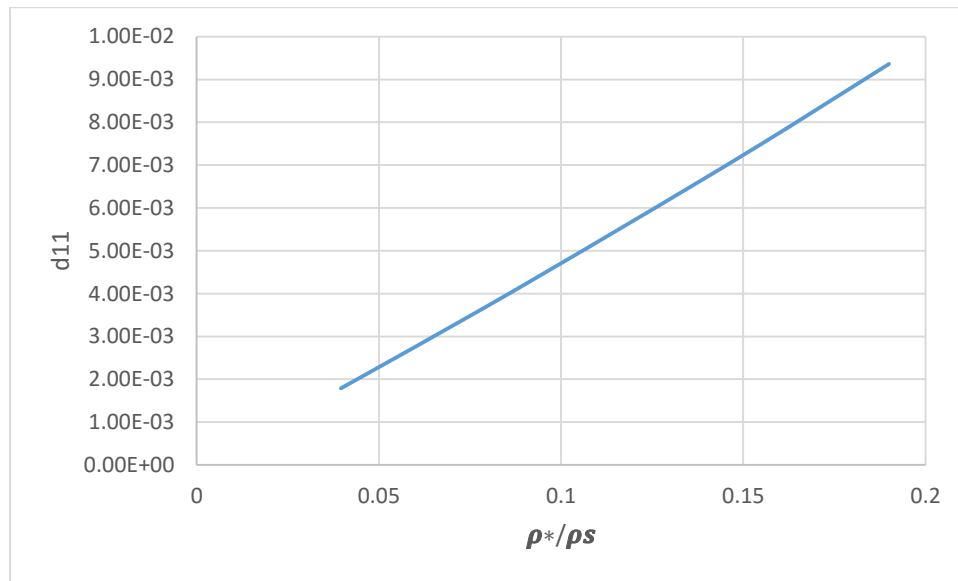


Figure 4.15. The  $d_{11}$  coefficient for the square honeycomb

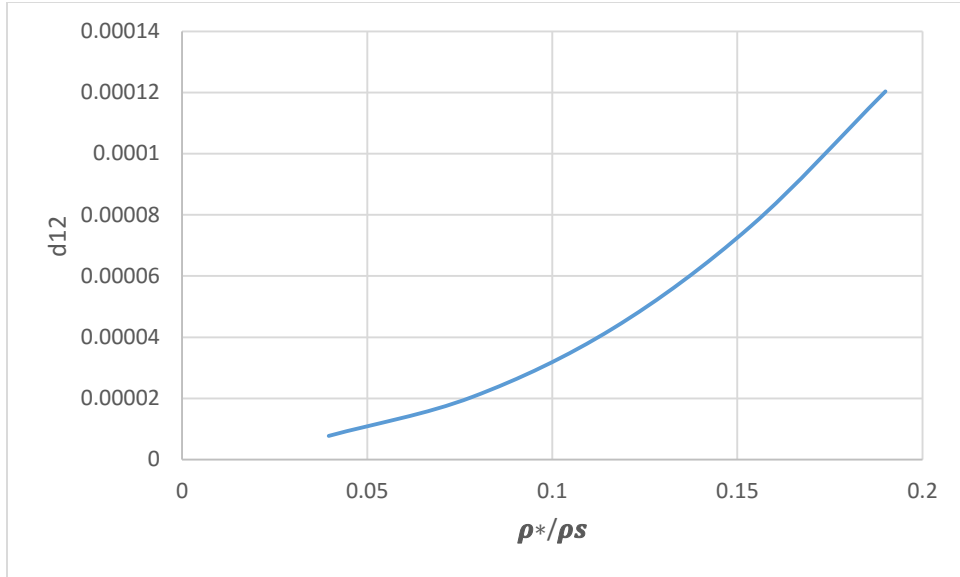


Figure 4.16. The  $d_{12}$  coefficient for the square honeycomb

For the equilateral triangular honeycombs, the results are shown in the following table and figures.

Table 16. Piezomagnetic coefficients for the triangular honeycombs (N/Am)

$t/l$	$d_{11}$	$d_{12}$	$d_{21}$	$d_{22}$
0.02	0.005814	0.004363	0.000821	0.010734
0.04	0.011172	0.005531	0.001521	0.01303
0.06	0.017148	0.006933	0.002507	0.016225
0.08	0.023315	0.008492	0.00366	0.020706
0.1	0.029419	0.009635	0.005107	0.023451

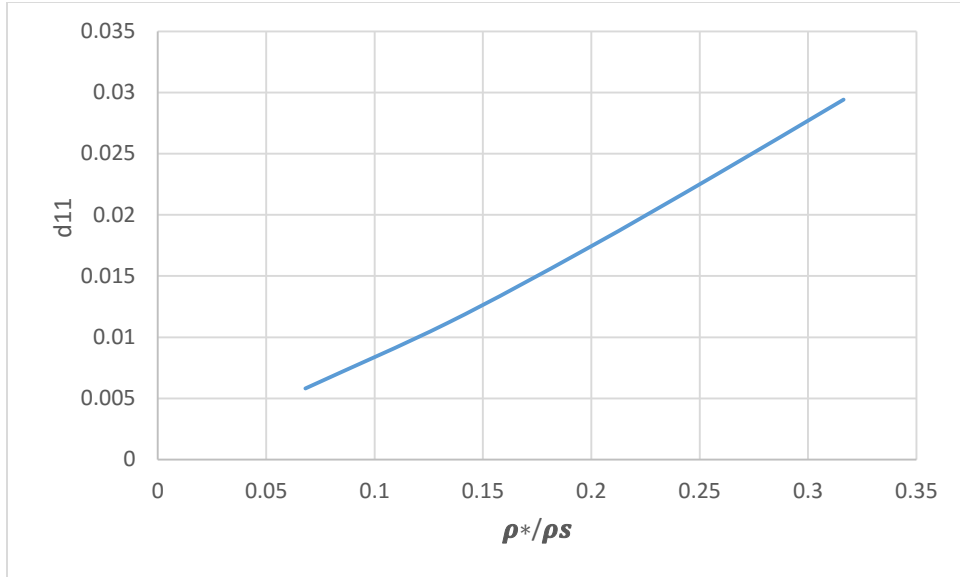


Figure 4.17. The  $d_{11}$  coefficient for the triangular honeycomb

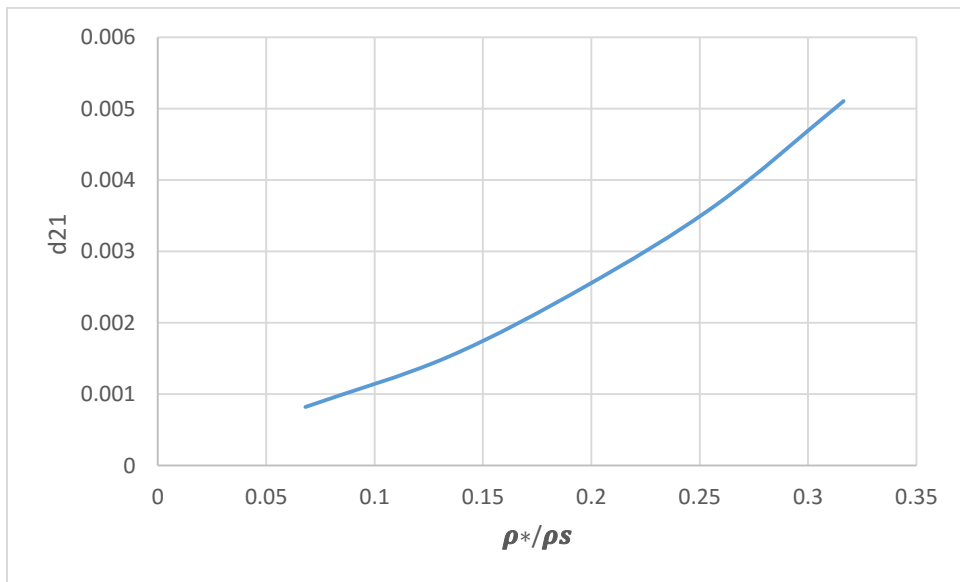


Figure 4.18 The  $d_{21}$  coefficient for the triangular honeycomb

For the hexagonal unit cells, all the results for the piezoelectric coefficients were non-linear and can be seen in Table 17 and the Figures 4.19 and 4.20.

Table 17. Piezomagnetic coefficients for the hexagonal honeycombs in (N/Am)

$t/l$	$d_{11}$	$d_{12}$	$d_{21}$	$d_{22}$
0.02	0.020111	-0.00344	0.00322	0.026467
0.04	0.107548	-0.01781	0.018692	0.139924
0.06	0.147896	-0.02346	0.027264	0.190579
0.08	0.184724	-0.02733	0.034942	0.23563
0.1	0.205444	-0.02813	0.039153	0.260095

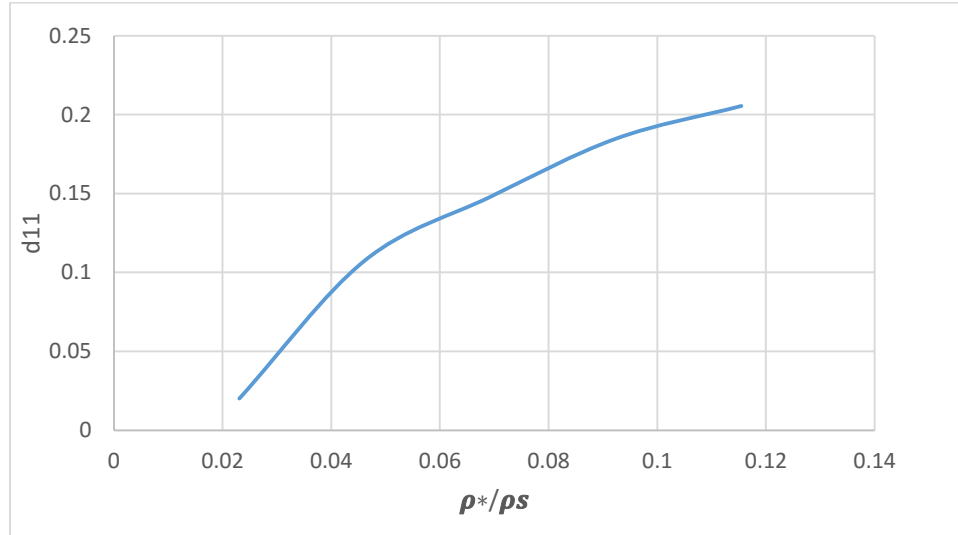


Figure 4.19: The  $d_{11}$  coefficient for the hexagonal honeycomb

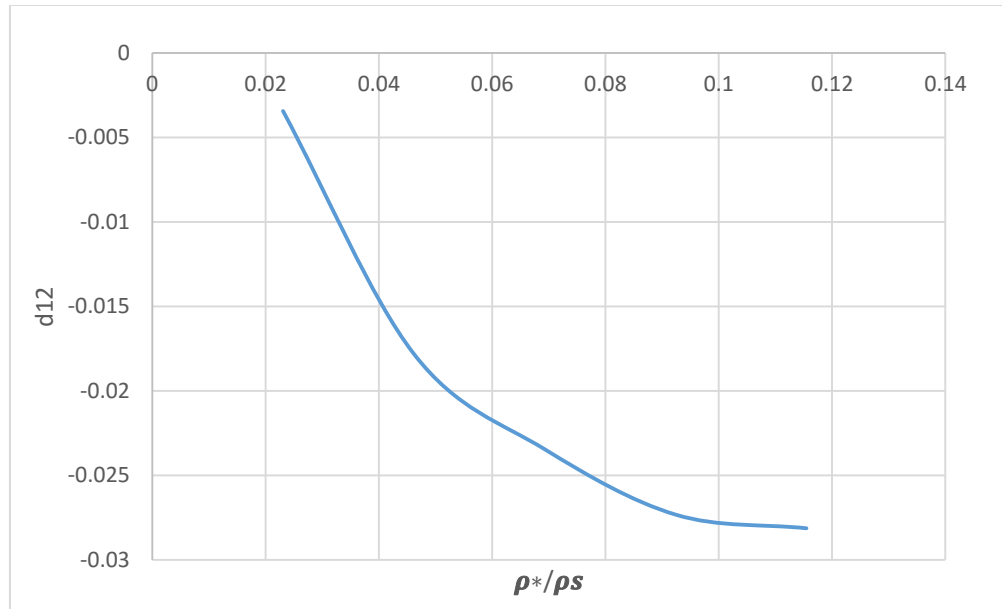


Figure 4.20. The  $d_{12}$  coefficient for the hexagonal honeycomb

#### 4.5 The thermal expansion coefficient:

The thermal expansion coefficient was found for the square, equilateral triangle and the regular hexagon unit cells and for the different values of (t/l) ratio. It has been found that the thermal expansion coefficient for all the cases has the same value of  $(1.95 \cdot 10^{-5} \frac{1}{K})$ , concluding that the thermal expansion coefficient is independent from the cell shapes and from the ratio of (t/l). This finding agrees with what can be found in Gibson and Ashby (1997) which addresses that the thermal expansion coefficient is almost the same as the material that the cellular solid is made from and it is in the range of  $(10^{-5} \frac{1}{K})$  for metals and that agrees with what has been found in this study. There was no need for any additional plots for this result.

#### 4.6 The effective pyroelectric and pyromagnetic properties:

The effective pyroelectric and pyromagnetic have the same characterization as the effective piezoelectric and the effective piezomagnetic coefficients since they are simply multiplied by the thermal expansion coefficient. The results are shown in the following figures and tables.

Table 18. The effective pyroelectric and pyromagnetic for the square honeycomb.  $\gamma$  in (C/Km<sup>2</sup>) and  $\tau$  in (N/AmK)

t/l	$\gamma_1$	$\gamma_2$	$\tau_1$	$\tau_2$
0.02	1.48018E-09	1.48E-09	3.49E-08	3.49E-08
0.04	3.02051E-09	3.02E-09	7.1E-08	7.1E-08
0.06	4.59432E-09	4.59E-09	1.08E-07	1.08E-07
0.08	6.18128E-09	6.18E-09	1.45E-07	1.45E-07
0.1	7.98634E-09	7.99E-09	1.83E-07	1.83E-07

Table 19. The effective pyroelectric and pyromagnetic for the triangular honeycomb.  $\gamma$  in (C/Km<sup>2</sup>) and  $\tau$  in (N/AmK)

t/l	$\gamma_1$	$\gamma_2$	$\tau_1$	$\tau_2$
0.02	6.07E-09	2.49E-09	1.13E-07	2.09E-07
0.04	1.17E-08	4.42E-09	2.18E-07	2.54E-07
0.06	1.79E-08	6.61E-09	3.34E-07	3.16E-07
0.08	2.4E-08	8.97E-09	4.55E-07	4.04E-07
0.1	3.02E-08	1.13E-08	5.74E-07	4.57E-07

Table 20. The effective pyroelectric and pyromagnetic for the hexagonal honeycomb.  $\gamma$  in (C/Km<sup>2</sup>) and  $\tau$  in (N/AmK)

t/l	$\gamma_1$	$\gamma_2$	$\tau_1$	$\tau_2$
0.02	2.31E-08	3.24E-08	3.92E-07	5.16E-07
0.04	1.23E-07	1.67E-07	2.1E-06	2.73E-06
0.06	1.67E-07	2.22E-07	2.88E-06	3.72E-06
0.08	2.07E-07	2.67E-07	3.6E-06	4.59E-06
0.1	2.28E-07	2.87E-07	4.01E-06	5.07E-06

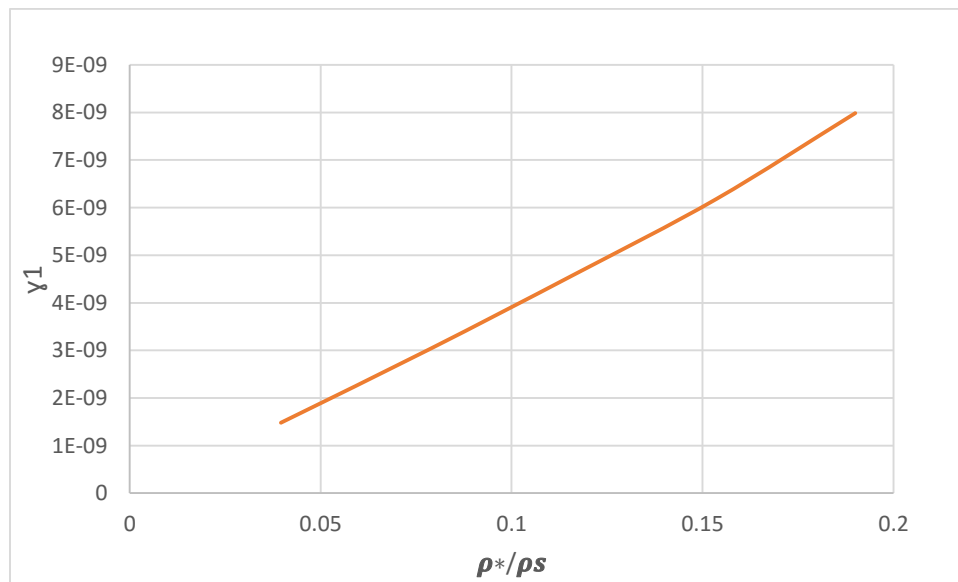


Figure 4.21. The  $\gamma_1$  coefficient for the square honeycomb

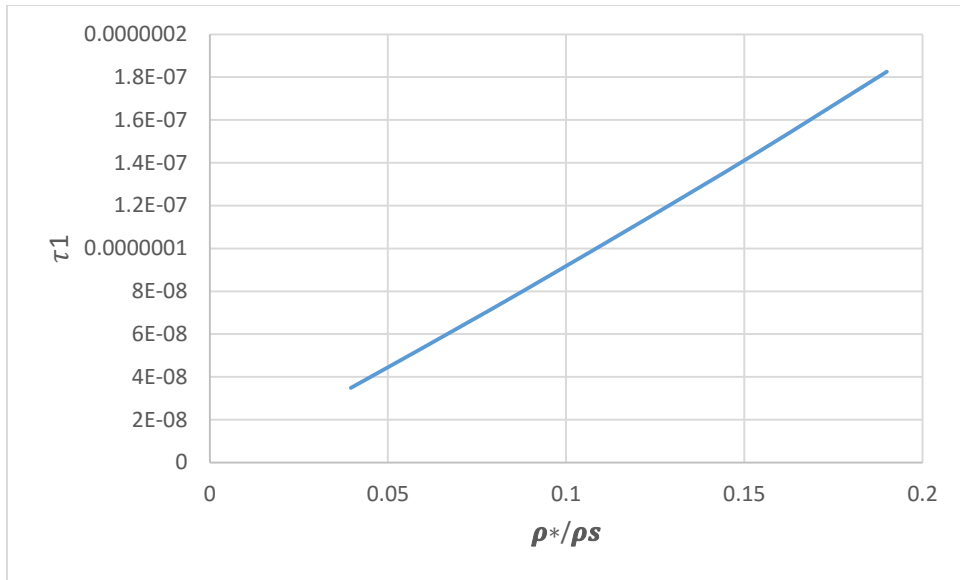


Figure 4.22. The  $\tau_1$  coefficient for the square honeycomb

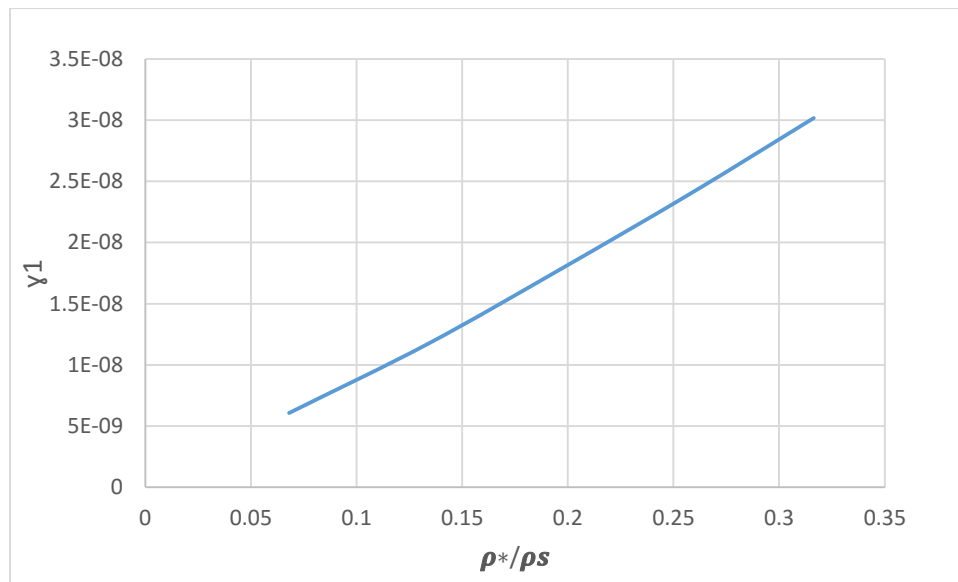


Figure 4.23. The  $\gamma_1$  coefficient for the triangular honeycomb

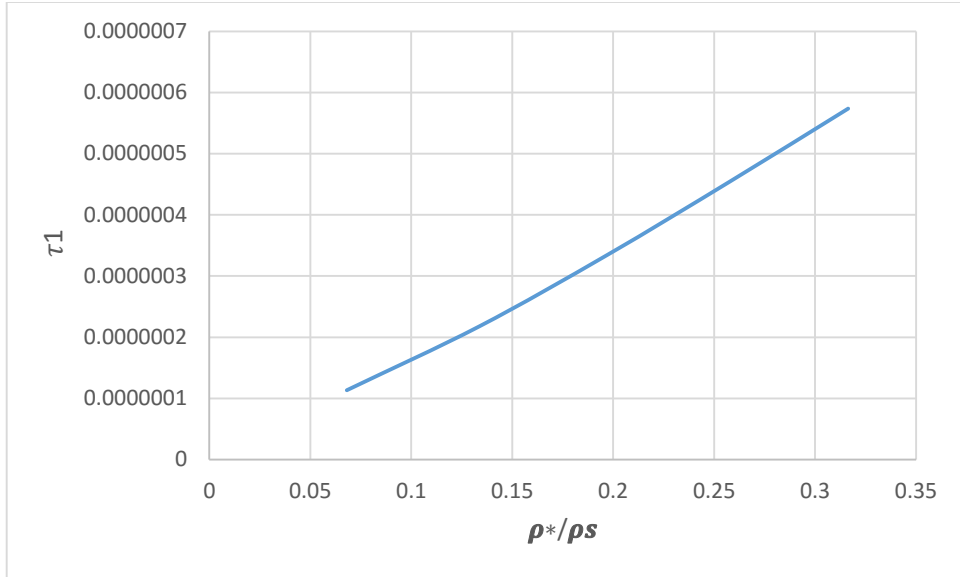
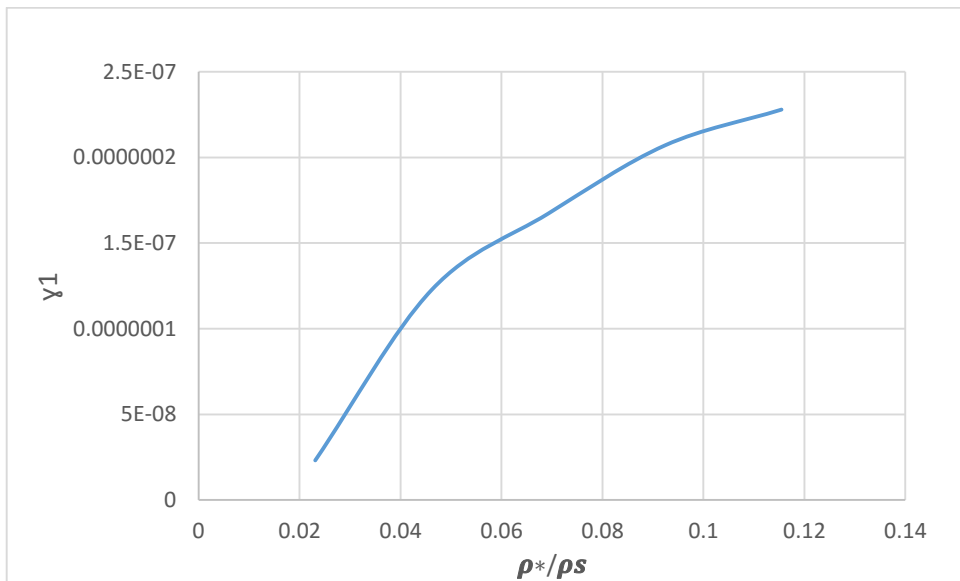
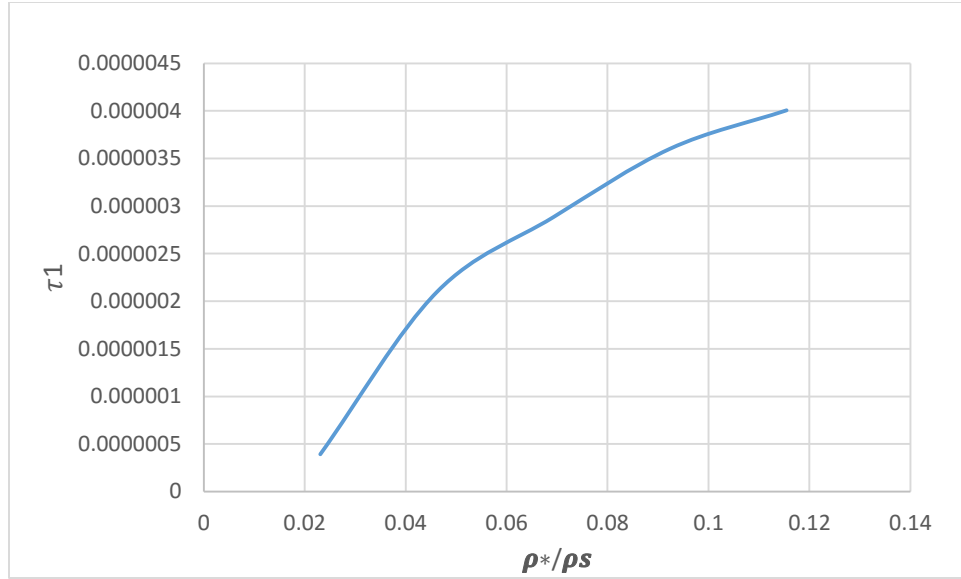


Figure 4.24. The  $\tau_1$  coefficient for the triangular honeycomb



4.25. The  $\gamma_1$  coefficient for the hexagonal honeycomb



4.26. The  $\tau_1$  coefficient for the hexagonal honeycomb

#### 4.7 Suggested equations for the effective properties

Simple equations are suggested to represent all the effective properties of the MEE cellular solid in terms of the relative density found by equations 3.55, 3.56 and 3.57 . The equations are shown below:

For the square honeycomb:

$$\frac{c_{11}}{c_{11m}} = \frac{c_{22}}{c_{22m}} = 0.4133 \left( \frac{\rho^*}{\rho_s} \right) \quad 4.6$$

$$\frac{c_{12}}{c_{12m}} = \frac{c_{21}}{c_{21m}} = 0.2627 \left( \frac{\rho^*}{\rho_s} \right)^{1.8958} \quad 4.7$$

$$\frac{c_{66}}{c_{66m}} = 0.91 \left( \frac{\rho^*}{\rho_s} \right) \quad 4.8$$

$$\frac{e_{11}}{e_{11m}} = \frac{e_{22}}{e_{22m}} = 0.0002 \left( \frac{\rho^*}{\rho_s} \right) \quad 4.9$$

$$\frac{e_{12}}{e_{12m}} = \frac{e_{21}}{e_{21m}} = 5 * 10^{-5} \left( \frac{\rho^*}{\rho_s} \right)^3 - 3 * 10^{-6} \left( \frac{\rho^*}{\rho_s} \right)^2 - 7 * 10^{-8} \left( \frac{\rho^*}{\rho_s} \right) \quad 4.10$$

$$\frac{d_{11}}{d_{11m}} = \frac{d_{22}}{d_{22m}} = 0.0002 \left( \frac{\rho^*}{\rho_s} \right) \quad 4.11$$

$$\frac{d_{12}}{d_{12m}} = \frac{d_{21}}{d_{21m}} = 10^{-5} \left( \frac{\rho^*}{\rho_s} \right)^3 + 9 * 10^{-6} \left( \frac{\rho^*}{\rho_s} \right)^2 - 7 * 10^{-8} \left( \frac{\rho^*}{\rho_s} \right) \quad 4.12$$

$$\frac{y_1}{y_{1m}} = \frac{y_2}{y_{2m}} = -0.0003 \left( \frac{\rho^*}{\rho_s} \right) \quad 4.13$$

$$\frac{\tau_1}{\tau_{1m}} = \frac{\tau_2}{\tau_{2m}} = 0.0002 \left( \frac{\rho^*}{\rho_s} \right) \quad 4.14$$

For the triangle honeycomb:

$$\frac{c_{11}}{c_{11m}} = \frac{c_{22}}{c_{22m}} = 0.3951 \left( \frac{\rho^*}{\rho_s} \right) \quad 4.15$$

$$\frac{c_{12}}{c_{12m}} = \frac{c_{21}}{c_{21m}} = 0.3582 \left( \frac{\rho^*}{\rho_s} \right) \quad 4.16$$

$$\frac{e_{11}}{e_{11m}} = 0.0006 \left( \frac{\rho^*}{\rho_s} \right) \quad 4.17$$

$$\frac{e_{12}}{e_{12m}} = 0.0001 \left( \frac{\rho^*}{\rho_s} \right)^3 - 0.0001 \left( \frac{\rho^*}{\rho_s} \right)^2 + 2 * 10^{-5} \left( \frac{\rho^*}{\rho_s} \right) \quad 4.18$$

$$\frac{e_{21}}{e_{21m}} = -0.0001 \left(\frac{\rho^*}{\rho_s}\right)^3 + 8 * 10^{-5} \left(\frac{\rho^*}{\rho_s}\right)^2 - 2 * 10^{-5} \left(\frac{\rho^*}{\rho_s}\right) \quad 4.19$$

$$\frac{e_{22}}{e_{22m}} = 0.0002 \left(\frac{\rho^*}{\rho_s}\right) \quad 4.20$$

$$\frac{d_{11}}{d_{11m}} = 0.0003 \left(\frac{\rho^*}{\rho_s}\right) \quad 4.21$$

$$\frac{d_{12}}{d_{12m}} = -0.0007 \left(\frac{\rho^*}{\rho_s}\right)^3 + 0.0005 \left(\frac{\rho^*}{\rho_s}\right)^2 - 10^{-5} \left(\frac{\rho^*}{\rho_s}\right) \quad 4.22$$

$$\frac{d_{21}}{d_{21m}} = 0.0001 \left(\frac{\rho^*}{\rho_s}\right)^2 + 10^{-5} \left(\frac{\rho^*}{\rho_s}\right) \quad 4.23$$

$$\frac{d_{22}}{d_{22m}} = -0.003 \left(\frac{\rho^*}{\rho_s}\right)^3 + 0.0019 \left(\frac{\rho^*}{\rho_s}\right)^2 - 0.0002 \left(\frac{\rho^*}{\rho_s}\right) \quad 4.24$$

$$\frac{y_1}{y_{1m}} = -0.0007 \left(\frac{\rho^*}{\rho_s}\right) \quad 4.25$$

$$\frac{y_2}{y_{2m}} = -0.0003 \left(\frac{\rho^*}{\rho_s}\right) \quad 4.26$$

$$\frac{\tau_1}{\tau_{1m}} = 0.0003 \left(\frac{\rho^*}{\rho_s}\right) \quad 4.27$$

$$\frac{\tau_2}{\tau_{2m}} = -0.0028 \left(\frac{\rho^*}{\rho_s}\right)^3 + 0.0018 \left(\frac{\rho^*}{\rho_s}\right)^2 - 0.0002 \left(\frac{\rho^*}{\rho_s}\right) \quad 4.28$$

For the hexagonal honeycomb:

$$\frac{c_{11}}{c_{11m}} = \frac{c_{22}}{c_{22m}} = 1483.2 \left(\frac{\rho^*}{\rho_s}\right)^3 - 434.9 \left(\frac{\rho^*}{\rho_s}\right)^2 + 49.817 \left(\frac{\rho^*}{\rho_s}\right) \quad 4.29$$

$$\frac{c_{12}}{c_{12m}} = \frac{c_{21}}{c_{21m}} = 2796 \left(\frac{\rho^*}{\rho_s}\right)^3 - 820.25 \left(\frac{\rho^*}{\rho_s}\right)^2 + 93.928 \left(\frac{\rho^*}{\rho_s}\right) \quad 4.30$$

$$\frac{e_{11}}{e_{11m}} = 1.4211 \left(\frac{\rho^*}{\rho_s}\right)^3 + 0.4211 \left(\frac{\rho^*}{\rho_s}\right)^2 + 0.0477 \left(\frac{\rho^*}{\rho_s}\right) \quad 4.31$$

$$\frac{e_{12}}{e_{12m}} = -1.2701 \left(\frac{\rho^*}{\rho_s}\right)^3 + 0.3709 \left(\frac{\rho^*}{\rho_s}\right)^2 - 0.0386 \left(\frac{\rho^*}{\rho_s}\right) \quad 4.32$$

$$\frac{e_{21}}{e_{21m}} = 1.3 \left(\frac{\rho^*}{\rho_s}\right)^3 - 0.3858 \left(\frac{\rho^*}{\rho_s}\right)^2 + 0.0438 \left(\frac{\rho^*}{\rho_s}\right) \quad 4.33$$

$$\frac{e_{22}}{e_{22m}} = 2.1835 \left(\frac{\rho^*}{\rho_s}\right)^3 - 0.6391 \left(\frac{\rho^*}{\rho_s}\right)^2 + 0.0684 \left(\frac{\rho^*}{\rho_s}\right) \quad 4.34$$

$$\frac{d_{11}}{d_{11m}} = 0.7179 \left(\frac{\rho^*}{\rho_s}\right)^3 - 0.212 \left(\frac{\rho^*}{\rho_s}\right)^2 + 0.0244 \left(\frac{\rho^*}{\rho_s}\right) \quad 4.35$$

$$\frac{d_{12}}{d_{12m}} = -0.1313 \left(\frac{\rho^*}{\rho_s}\right)^3 + 0.0406 - 0.0044 \left(\frac{\rho^*}{\rho_s}\right) \quad 4.36$$

$$\frac{d_{21}}{d_{21m}} = 0.0796 \left(\frac{\rho^*}{\rho_s}\right)^3 - 0.0273 \left(\frac{\rho^*}{\rho_s}\right)^2 + 0.0038 \left(\frac{\rho^*}{\rho_s}\right) \quad 4.37$$

$$\frac{d_{22}}{d_{22m}} = 0.9782 \left(\frac{\rho^*}{\rho_s}\right)^3 - 0.2875 \left(\frac{\rho^*}{\rho_s}\right)^2 + 0.0323 \left(\frac{\rho^*}{\rho_s}\right) \quad 4.38$$

$$\frac{y_1}{y_{1m}} = -1.8886 \left(\frac{\rho^*}{\rho_s}\right)^3 + 0.5597 \left(\frac{\rho^*}{\rho_s}\right)^2 - 0.0634 \left(\frac{\rho^*}{\rho_s}\right) \quad 4.39$$

$$\frac{y_2}{y_{2m}} = -2.9019 \left(\frac{\rho^*}{\rho_s}\right)^3 + 0.8493 \left(\frac{\rho^*}{\rho_s}\right)^2 - 0.0909 \left(\frac{\rho^*}{\rho_s}\right) \quad 4.40$$

$$\frac{\tau_1}{\tau_{1m}} = 0.6813 \left(\frac{\rho^*}{\rho_s}\right)^3 - 0.2012 \left(\frac{\rho^*}{\rho_s}\right)^2 + 0.0231 \left(\frac{\rho^*}{\rho_s}\right) \quad 4.41$$

$$\frac{\tau_2}{\tau_{2m}} = 0.9283 \left(\frac{\rho^*}{\rho_s}\right)^3 - 0.2729 \left(\frac{\rho^*}{\rho_s}\right)^2 + 0.0307 \left(\frac{\rho^*}{\rho_s}\right) \quad 4.42$$

## CHAPTER 5: SUMMARY AND CONCLUSION

A finite element study was conducted to find the effective elastic, piezoelectric, piezomagnetic, pyroelectric and pyromagnetic properties for three shapes of two-dimensional cellular solid made from MEE material.

### 5.1 Conclusions:

The primary conclusions of the present study are as follows:

1. The results of the elastic properties showed that the equilateral triangular honeycombs are the stiffest among all the honeycombs shapes. For the same  $(t/l)$  ratio, it has a value of the elastic modulus higher than the elastic modulus for the square honeycomb by a factor of (1.27) and higher than the hexagonal honeycomb by an average factor of (386) and that shows that the hexagonal honeycomb is the most flexible by large difference.
2. The elastic properties found in this study were slightly higher than those found by other studies and this influences and the other properties that have been found in this study. In all likelihood, this is caused by the inclusion of the full equations of elasticity rather than approximations based on bar or beam theory of several other models.
3. As originally stated by Gibson and Ashby (reference), the effective thermal expansion coefficient is constant and independent from the  $(t/l)$  ratio and the relative density for all the cell shapes of the honeycombs.

4. All the piezoelectric, piezomagnetic, pyroelectric and pyromagnetic increased in magnitude with the increase of the relative density according to a fairly simple polynomial law.
5. The piezoelectric coefficients of the hexagonal honeycombs showed the highest values compared to those of other shapes. For example, the piezoelectric coefficient  $e_{11}$  for the regular hexagons is higher than  $e_{11}$  for the triangle by an average of (8) times and higher than the square coefficient by a factor of (31)
6. For the square honeycomb, all the piezoelectric coefficients were positive, leading to a decrease in both dimensions of the honeycomb when an electric potential is applied. For the triangular or the hexagonal honeycombs, negative effective piezoelectric coefficients were obtained.
7. For the piezomagnetic coefficient, the hexagonal honeycombs again showed the highest values of the piezomagnetic coefficient between the other shapes. For example, the piezomagnetic coefficient  $d_{11}$  for the regular hexagons is higher than  $d_{11}$  for the triangle by an average of (7) times and higher than the square coefficient by (22) times.
8. All the piezomagnetic coefficients for the square and triangular honeycombs were positive. The piezomagnetic coefficient  $d_{12}$  for the regular hexagon was the only negative coefficient between all the piezomagnetic coefficients.
9. The pyroelectric and pyromagnetic coefficients have the same behavior as the piezoelectric and the piezomagnetic coefficients. The hexagonal honeycomb showed the highest values.

10. The hexagonal honeycomb is the most flexible of the three configurations studied and has the highest values of the effective piezoelectric, piezomagnetic, pyroelectric and pyromagnetic properties.

## 5.2 Future work:

1. Other shapes with a negative Poisson's ratio can be explored including the inverted hexagonal honeycomb with ( $\theta = -30$ ). A total different behavior of the other properties can be obtained due to the auxetic behavior of these shapes.
2. Effect of irregularities and defects such as missing cell walls or the effect of thickness variations can be investigated. The use of the repeating unit cell is invalid for this case and a representative volume element should be used. The size of RVE will affect the properties and a new set of equations should be presented.
3. Three-dimensional cellular solids (foams) made from MEE material can be studied. A new set of equations can be presented by studying the unit cells for the foams used in Gibson and Ashby (1997) or any other shapes that have been studied by others.
4. Dynamic loading and free vibration of the MEE cellular solid can be investigated since most of the applications for the MEE materials, such as structural health monitoring and energy harvesting, are dealing with dynamic loads.
5. Non-steady transient problem can be studied where all the variables are time dependent.
6. Post elastic behavior, buckling of the cell walls and crushing of the honeycomb can be considered in the future.

## REFERENCES

- [1] J. Aboudi, "Micromechanical analysis of fully coupled multiphase composites," *Smart Mater. Struct.*, vol. 10, pp. 867–877, 2001.
- [2] A. H. Akbarzadeh and Z. T. Chen, "Magneto-electroelastic behavior of rotating cylinders resting on an elastic foundation under hygrothermal loading," *Smart Mater. Struct.*, vol. 21, no. 12, p. 125013, Dec. 2012.
- [3] A. H. Akbarzadeh and D. Pasini, "Multiphysics of Multilayered and Functionally Graded Cylinders Under Prescribed Hygrothermomagneto-electromechanical Loading," *J. Appl. Mech.*, vol. 81, no. 4, p. 041018, Nov. 2013.
- [4] A. H. Akbarzadeh and Z. T. Chen, "Hygrothermal stresses in one-dimensional functionally graded piezoelectric media in constant magnetic field," *Compos. Struct.*, vol. 97, pp. 317–331, Mar. 2013.
- [5] M. F. Ashby, G. S. Schajer, and C. I. Robertson, "The mechanics of two-dimensional cellular materials," vol. 382, no. 1782, pp. 25–42, 2015.
- [6] D. N. ASTROV, *SoY. Phys JETP* 11, 708, 1960.
- [7] K. S. Challagulla, T. A. Venkatesh, and S. Brook, "Electromechanical response of piezoelectric foam." pp. 1–6.
- [8] J. Y. Chen, E. Pan, P.R. Heyliger, "Static deformation of a spherically and multilayered magneto-electro-elastic hollow sphere." *Int. J. solids struct.*, vol. 60-61, pp. 66-74, 2015.
- [9] J. Y. Chen, Heyliger, P. R., and Pan, E., "Free vibration of three-dimensional multilayered magneto- electro-elastic plates under combined clamped/free boundary conditions," *Journal of Sound and Vibration* 333, pp. 4017-4029, 2014.
- [10] C. Chen, T. J. Lu, and N. A. Fleck, "Effect of imperfections on the yielding of two-dimensional foams," *Mech. Mech. Phys. solids*, vol. 47, pp. 2235–2272, 1999.
- [11] R. M. Christensen, "Mechanics of cellular and other low-density materials," *Int. J. Solids Struct.*, vol. 37, no. 1–2, pp. 93–104, Jan. 2000.
- [12] M. L. Dunn and M. Taya, "Electromechanical Properties of Porous Piezoelectric Ceramics," *J. Am. Ceram. Soc.*, vol. 76, no. 7, pp. 1697–1706, 1993.
- [13] L. J. Gibson, Ashby, M. F. "*Cellular solids: Structure and properties.*" 2nd ed. Cambridge: Cambridge University Press, 1997.
- [14] L. j. Gibson, "Modelling the Mechanical Behavior of Cellular Materials," *Mater. Sci. Eng.*, vol. 110, pp. 1–36, 1989.
- [15] S. T. Gulati. Paper 750151, Automotive Engineering Congress and Exhibition Society of Automotive engineers, Detroit, Michigan, 24-28 February, P. 157, 1975

- [16] G. Harshe, Dougherty, J.P., Newnham, R.E., "Theoretical modelling of 3–0/0–3 magnetoelectric composites." *Int. J. Appl. Electromagn. Mater.* 4, 161–171, 1993.
- [17] P.R. Heyliger, and R.M. McMeeking, "Cold Plastic Compaction of Powders by a Network Model," *J. Mechanics and Physics of Solids*, vol. 49, pp. 2031-2054, 2001.
- [18] J. Hohe and W. Becker, "Effective mechanical behavior of hyperelastic honeycombs and two-dimensional model foams at finite strain," *Int. J. Mech. Sci.*, vol. 45, no. 5, pp. 891–913, May 2003.
- [19] G.-Y. Huang, B.-L. Wang, and Y.-W. Mai, "Effective properties of magneto-electroelastic materials with aligned ellipsoidal voids," *Mech. Res. Commun.*, vol. 36, no. 5, pp. 563–572, Jul. 2009.
- [20] Hunt, H. E. M. 'The mechanical strength of ceramic honeycomb monoliths as determined by simple experiments': *Advanced materials. Chemical engineering research & design*, 71(3), 257-266.1993.
- [21] S. Iyer, M. Alkhader, and T. a. Venkatesh, "Electromechanical Response of Piezoelectric Honeycomb Foam Structures," *J. Am. Ceram. Soc.*, vol. 97, no. 3, pp. 826–834, Mar. 2014.
- [22] S. Iyer and T. a. Venkatesh, "Electromechanical response of (3–0,3–1) particulate, fibrous, and porous piezoelectric composites with anisotropic constituents: A model based on the homogenization method," *Int. J. Solids Struct.*, vol. 51, no. 6, pp. 1221–1234, Mar. 2014.
- [23] Emery James D., Piezoelectricity, Unpublished Document. 1997.
- [24] Y. L. Jiang and L. D. Martin, "Micromechanics of Magneto-electroelastic Composite Average Fields and Effective Behavior," *Intell. Mater. Syst. Struct.*, vol. 9, pp. 404–416, 1998.
- [25] R. C. Kambale, D.-Y. Jeong, and J. Ryu, "Current Status of Magneto-electric Composite Thin/Thick Films," *Adv. Condens. Matter Phys.*, vol. 2012, pp. 1–15, 2012.
- [26] K. Li, X.-L. Gao, and G. Subhash, "Effects of cell shape and cell wall thickness variations on the elastic properties of two-dimensional cellular solids," *Int. J. Solids Struct.*, vol. 42, no. 5–6, pp. 1777–1795, Mar. 2005.
- [27] L. D. Landau, and Lifshitz, E. M., "Electrodynamics of Continuous Media, 2nd Ed.," Rev. and Enlarged by E. M. Lifshitz and L. P. Pitaevskii, Pergamon Press, New York, 1984.
- [28] C. Nan, "Product property between thermal expansion and piezoelectricity in piezoelectric composites " pyroelectricity," *Mater. Sci.*, vol. 13, pp. 1392–1394, 1994.
- [29] C.-W. Nan, M. I. Bichurin, S. Dong, D. Viehland, and G. Srinivasan, "Multiferroic magneto-electric composites: Historical perspective, status, and future directions," *J. Appl. Phys.*, vol. 103, no. 3, p. 031101, 2008.
- [30] E. Pan, "Exact Solution for Simply Supported and Multilayered Magneto-Electro-Elastic Plates," *J. Appl. Mech.*, vol. 68, no. 4, p. 608, 2001.

- [31] E. Pan and P. R. Heyliger, "Free Vibrations of Simply Supported and Multilayered Magneto-Electro-Elastic Plates," *J. Sound Vib.*, vol. 252, no. 3, pp. 429–442, May 2002.
- [32] M.-J. Pindera, H. Khatam, A. S. Drago, and Y. Bansal, "Micromechanics of spatially uniform heterogeneous media: A critical review and emerging approaches," *Compos. Part B Eng.*, vol. 40, no. 5, pp. 349–378, Jul. 2009.
- [33] F. Ramirez, P. R. Heyliger, and E. Pan, "Free vibration response of two-dimensional magneto-electro-elastic laminated plates," *J. Sound Vib.*, vol. 292, no. 3–5, pp. 626–644, May 2006.
- [34] J.N. Reddy, "An Introduction to the Finite Element Method," Third Edition, McGraw-Hill, NY, 2006.
- [35] Richard M. Christensen, "Effective properties of composite materials containing voids," *Math. Phys. Sci.*, vol. 440, pp. 461–473, 1993.
- [36] J. Steadman, Atadero, R. A., and Heyliger, P. R., "Influence of Local Wall Variation in the Elastic Properties of Planar Cellular Solids," *Mechanics of Advanced Materials and Structures* 21, pp. 117-128, 2014.
- [37] M. J. Silva and L. J. Gibson, "The effects of non-periodic microstructure and defects on the compressive strength of two-dimensional cellular solids," *Int. J. Mech. Sci.*, vol. 39, no. 5, pp. 549–563, May 1997.
- [38] M. J. Silva, W. C. Hayes, and L. J. Gibson, "The Effects of Non-periodic Microstructure on the Elastic properties of Two-Dimensional Cellular solids," *Int. J. Mech. Sci.*, vol. 37, no. 11, pp. 1161–1177, 1995.
- [39] W. Smittakorn and P.R. Heyliger, "A Discrete Layer Model of Hygrothermopiezoelectric Plates," *Mechanics of Composite Materials and Structures*, Vol. 7, pp. 79-104, 2000.
- [40] K. H. Sun and Y. Y. Kim, "Layout design optimization for magneto-electro-elastic laminate composites for maximized energy conversion under mechanical loading," *Smart Mater. Struct.*, vol. 19, no. 5, p. 055008, May 2010.
- [41] J. A. Steadman, "Modeling the elastic properties of two-dimensional cellular solids." Master's Thesis. Colorado State University, Fort Collins, CO, 2009.
- [42] C. M. Taylor, C. W. Smith, W. Miller, and K. E. Evans, "The effects of hierarchy on the in-plane elastic properties of honeycombs," *Int. J. Solids Struct.*, vol. 48, no. 9, pp. 1330–1339, May 2011.
- [43] a. M. J. G. Van Run, D. R. Terrell, and J. H. Scholing, "An in situ grown eutectic magnetoelectric composite material," *J. Mater. Sci.*, vol. 9, no. 10, pp. 1710–1714, Oct. 1974.
- [44] J. VanSuchtelen, "Product properties: a new application of composite materials," *Philips Research Reports* 27, 28–37, 1972.

- [45] W. E. Warren and A. M. Kraynik, "Foam Mechanics: The Linear Elastic Response of Two-Dimensional Spatially Periodic Cellular Materials," *Mech. Mater.*, vol. 6, pp. 27–37, 1987.
- [46] a. M. Zenkour, "Hygrothermoelastic responses of inhomogeneous piezoelectric and exponentially graded cylinders," *Int. J. Press. Vessel. Pip.*, vol. 119, pp. 8–18, Jul. 2014.
- [47] Z. Zhang and X. Wang, "Effective multi-field properties of electro-magneto-thermoelastic composites estimated by finite element method approach," *Acta Mech. Solida Sin.*, vol. 28, no. 2, pp. 145–155, Apr. 2015.
- [48] j. Van Den BO, "A sintered magnetolectric composite material BaTiO<sub>3</sub>-Ni ( Co . Mn ) Fe<sub>2</sub>O<sub>4</sub>," *Mater. Sci.*, vol. 13, pp. 1538–1548, 1978.

## APPENDIX A: ELEMENTS OF THE MATRIX EQUATIONS FOR THE RITZ MODEL

$$K_{i,j}^{11} = \int_A [c_{11} \frac{\partial N_i^u}{\partial x} \frac{\partial N_j^u}{\partial x} + c_{16} (\frac{\partial N_i^u}{\partial x} \frac{\partial N_j^u}{\partial y} + \frac{\partial N_i^u}{\partial y} \frac{\partial N_j^u}{\partial x}) + c_{66} \frac{\partial N_i^u}{\partial y} \frac{\partial N_j^u}{\partial y}] dx dy \quad (A1)$$

$$K_{i,j}^{12} = \int_A [c_{12} \frac{\partial N_i^u}{\partial x} \frac{\partial N_j^v}{\partial y} + c_{16} \frac{\partial N_i^u}{\partial x} \frac{\partial N_j^v}{\partial x} + c_{26} \frac{\partial N_i^u}{\partial y} \frac{\partial N_j^v}{\partial y} + c_{66} \frac{\partial N_i^u}{\partial y} \frac{\partial N_j^v}{\partial x}] dx dy \quad (A2)$$

$$K_{i,j}^{13} = \int_A [e_{11} \frac{\partial N_i^u}{\partial x} \frac{\partial N_j^\phi}{\partial x} + e_{21} \frac{\partial N_i^u}{\partial x} \frac{\partial N_j^\phi}{\partial y} + e_{16} \frac{\partial N_i^u}{\partial y} \frac{\partial N_j^\phi}{\partial x} + e_{26} \frac{\partial N_i^u}{\partial y} \frac{\partial N_j^\phi}{\partial y}] dx dy \quad (A3)$$

$$K_{i,j}^{14} = \int_A [d_{11} \frac{\partial N_i^u}{\partial x} \frac{\partial N_j^\psi}{\partial x} + d_{21} \frac{\partial N_i^u}{\partial x} \frac{\partial N_j^\psi}{\partial y} + d_{16} \frac{\partial N_i^u}{\partial y} \frac{\partial N_j^\psi}{\partial x} + d_{26} \frac{\partial N_i^u}{\partial y} \frac{\partial N_j^\psi}{\partial y}] dx dy \quad (A4)$$

$$K_{i,j}^{15} = \int_A [-\beta_{11} \frac{\partial N_i^u}{\partial x} N_j^\theta - \beta_{12} \frac{\partial N_i^u}{\partial y} N_j^\theta] dx dy \quad (A5)$$

$$K_{i,j}^{16} = \int_A [-\zeta_{11} \frac{\partial N_i^u}{\partial x} N_j^m - \zeta_{12} \frac{\partial N_i^u}{\partial y} N_j^m] dx dy \quad (A6)$$

$$K_{i,j}^{21} = \int_A [c_{16} \frac{\partial N_i^v}{\partial x} \frac{\partial N_j^u}{\partial x} + c_{66} \frac{\partial N_i^v}{\partial x} \frac{\partial N_j^u}{\partial y} + c_{12} \frac{\partial N_i^v}{\partial y} \frac{\partial N_j^u}{\partial x} + c_{26} \frac{\partial N_i^v}{\partial y} \frac{\partial N_j^u}{\partial y}] dx dy \quad (A7)$$

$$K_{i,j}^{22} = \int_A [c_{26} \frac{\partial N_i^v}{\partial x} \frac{\partial N_j^v}{\partial y} + c_{66} \frac{\partial N_i^v}{\partial x} \frac{\partial N_j^v}{\partial x} + c_{22} \frac{\partial N_i^v}{\partial y} \frac{\partial N_j^v}{\partial y} + c_{26} \frac{\partial N_i^v}{\partial y} \frac{\partial N_j^v}{\partial x}] dx dy \quad (A8)$$

$$K_{i,j}^{23} = \int_A [e_{16} \frac{\partial N_i^v}{\partial x} \frac{\partial N_j^\phi}{\partial x} + e_{26} \frac{\partial N_i^v}{\partial x} \frac{\partial N_j^\phi}{\partial y} + e_{12} \frac{\partial N_i^v}{\partial y} \frac{\partial N_j^\phi}{\partial x} + e_{22} \frac{\partial N_i^v}{\partial y} \frac{\partial N_j^\phi}{\partial y}] dx dy \quad (A9)$$

$$K_{i,j}^{24} = \int_A [d_{16} \frac{\partial N_i^v}{\partial x} \frac{\partial N_j^\psi}{\partial x} + d_{26} \frac{\partial N_i^v}{\partial x} \frac{\partial N_j^\psi}{\partial y} + d_{12} \frac{\partial N_i^v}{\partial y} \frac{\partial N_j^\psi}{\partial x} + d_{22} \frac{\partial N_i^v}{\partial y} \frac{\partial N_j^\psi}{\partial y}] dx dy \quad (A10)$$

$$K_{i,j}^{25} = \int_A [-\beta_{12} \frac{\partial N_i^v}{\partial x} N_j^\theta - \beta_{22} \frac{\partial N_i^v}{\partial y} N_j^\theta] dx dy \quad (A11)$$

$$K_{i,j}^{26} = \int_A [-\zeta_{12} \frac{\partial N_i^v}{\partial x} N_j^m - \zeta_{22} \frac{\partial N_i^v}{\partial y} N_j^m] dx dy \quad (A12)$$

$$K_{i,j}^{33} = \int_A [-\varepsilon_{11} \frac{\partial N_i^\phi}{\partial x} \frac{\partial N_j^\phi}{\partial x} - \varepsilon_{12} \frac{\partial N_i^\phi}{\partial x} \frac{\partial N_j^\phi}{\partial y} - \varepsilon_{12} \frac{\partial N_i^\phi}{\partial y} \frac{\partial N_j^\phi}{\partial x} - \varepsilon_{22} \frac{\partial N_i^\phi}{\partial y} \frac{\partial N_j^\phi}{\partial y}] dx dy \quad (A13)$$

$$K_{i,j}^{34} = \int_A [-g_{11} \frac{\partial N_i^\phi}{\partial x} \frac{\partial N_j^\psi}{\partial x} - g_{12} \frac{\partial N_i^\phi}{\partial x} \frac{\partial N_j^\psi}{\partial y} - g_{12} \frac{\partial N_i^\phi}{\partial y} \frac{\partial N_j^\psi}{\partial x} - g_{22} \frac{\partial N_i^\phi}{\partial y} \frac{\partial N_j^\psi}{\partial y}] dx dy \quad (A14)$$

$$K_{i,j}^{36} = \int_A [\gamma_1 \frac{\partial N_i^\phi}{\partial x} N_j^m + \gamma_2 \frac{\partial N_i^\phi}{\partial y} N_j^m] dx dy \quad (A15)$$

$$K_{i,j}^{44} = \int_A [-\mu_{11} \frac{\partial N_i^\psi}{\partial x} \frac{\partial N_j^\psi}{\partial x} - \mu_{12} \frac{\partial N_i^\psi}{\partial x} \frac{\partial N_j^\psi}{\partial y} - \mu_{12} \frac{\partial N_i^\psi}{\partial y} \frac{\partial N_j^\psi}{\partial x} - \mu_{22} \frac{\partial N_i^\psi}{\partial y} \frac{\partial N_j^\psi}{\partial y}] dx dy \quad (A16)$$

$$K_{i,j}^{45} = \int_A [\tau_1 \frac{\partial N_i^\psi}{\partial x} N_j^\theta + \tau_2 \frac{\partial N_i^\psi}{\partial y} N_j^\theta] dx dy \quad (\text{A16})$$

$$K_{i,j}^{46} = \int_A [\nu_1 \frac{\partial N_i^\psi}{\partial x} N_j^m + \nu_2 \frac{\partial N_i^\psi}{\partial y} N_j^m] dx dy \quad (\text{A17})$$

$$K_{i,j}^{55} = \int_A [K_x^\theta \frac{\partial N_i^\theta}{\partial x} \frac{\partial N_j^\theta}{\partial x} + K_y^\theta \frac{\partial N_i^\theta}{\partial y} \frac{\partial N_j^\theta}{\partial y}] dx dy \quad (\text{A18})$$

$$K_{i,j}^{66} = \int_A [K_x^m \frac{\partial N_i^m}{\partial x} \frac{\partial N_j^m}{\partial x} + K_y^m \frac{\partial N_i^m}{\partial y} \frac{\partial N_j^m}{\partial y}] dx dy \quad (\text{A19})$$

## APPENDIX B: MATLAB CODE

```
% Multi Physics of MEE foam

% This program was written by Mustafa Khattab

% Last update 04/21/2015

% nem : # of elements

% Nnodes : # of nodes

% x,y : arrays/vectors of (x,y) pairs of each nodes x(nnodes), y(nnodes)

% nod : connectivity array (nem,4)

% nebs : # of EBC's

% nodebc : array that contains global d.o.f that are known

% valebc : array that contains values of EBC

% nNBC : # of NBC's

% nodNBC : array that contains global d.o.f that are known

% valNBC : array that contains values of NBC

clear all;

clc;

fem2ddata=xlsread('moisture');

nem = fem2ddata(1,1);

nnodes = fem2ddata(1,2);

nebc = fem2ddata(1,3);

nNBC = fem2ddata(1,4);

c11=fem2ddata(2,1);

c12=fem2ddata(2,2);

c22=fem2ddata(2,3);
```

c16=fem2ddata(2,4);  
c26=fem2ddata(2,5);  
c66=fem2ddata(2,6);  
e11=fem2ddata(3,1);  
e12=fem2ddata(3,2);  
e21=fem2ddata(3,3);  
e22=fem2ddata(3,4);  
e16=fem2ddata(3,5);  
e26=fem2ddata(3,6);  
e66=fem2ddata(3,7);  
d11=fem2ddata(4,1);  
d12=fem2ddata(4,2);  
d21=fem2ddata(4,3);  
d22=fem2ddata(4,4);  
d16=fem2ddata(4,5);  
d26=fem2ddata(4,6);  
d66=fem2ddata(4,7);  
beta11=fem2ddata(5,1);  
beta12=fem2ddata(5,2);  
beta22=fem2ddata(5,3);  
eps11=fem2ddata(6,1);  
eps12=fem2ddata(6,2);  
eps22=fem2ddata(6,3);  
mu11=fem2ddata(7,1);

```
mu12=fem2ddata(7,2);
mu22=fem2ddata(7,3);
g11=fem2ddata(8,1);
g12=fem2ddata(8,2);
g22=fem2ddata(8,3);
zeta11=fem2ddata(9,1);
zeta12=fem2ddata(9,2);
zeta22=fem2ddata(9,3);
gamma1=fem2ddata(10,1);
gamma2=fem2ddata(10,2);
tau1=fem2ddata(11,1);
tau2=fem2ddata(11,2);
nu1=fem2ddata(12,1);
nu2=fem2ddata(12,2);
kxt=fem2ddata(13,1);
kyt=fem2ddata(13,2);
kxm=fem2ddata(14,1);
kym=fem2ddata(14,2);
% Read in the (x,y) pairs
for i = 1: nnodes;
    x(i)=fem2ddata(i+14,2);
    y(i)=fem2ddata(i+14,3);
end
```

```

% Read in elements of connectivity array
for i=1:nem;

    nod(i,1)=fem2ddata(14+nnodes+i,2);

    nod(i,2)=fem2ddata(14+nnodes+i,3);

    nod(i,3)=fem2ddata(14+nnodes+i,4);

    nod(i,4)=fem2ddata(14+nnodes+i,5);

end

% % Read in all EBC Data

for i=1:nebc;

    nodebc(i)=fem2ddata(14+nnodes+nem+i,1);

    valebc(i)=fem2ddata(14+nnodes+nem+i,2);

end

% Read in the NBC Data

for i=1:n NBC;

    nodnbc(i)=fem2ddata(14+nnodes+nem+nebc+i,1);

    valnbc(i)=fem2ddata(14+nnodes+nem+nebc+i,2);

end

% Read in Gauss points and weights

gauss=zeros(4,4);

weight=zeros(4,4);

gauss(1,1)=0.0;

```

```
gauss(1,2)=0.57735;
gauss(2,2)=-0.57735;

gauss(1,3)=0.77459;
gauss(2,3)=0;
gauss(3,3)=-0.77459;
gauss(1,4)=0.33998;
gauss(2,4)=-0.33998;
gauss(3,4)=0.861136;
gauss(4,4)=-0.861136;

weight(1,1)=2;
weight(1,2)=1;
weight(2,2)=1;
weight(1,3)=0.555556;
weight(2,3)=0.888889;
weight(3,3)=0.555556;
weight(1,4)=0.65214;
weight(2,4)=0.65214;
weight(3,4)=0.3478;
weight(4,4)=0.3478;

% gauss/weight to start

% zero the global matrices
globalk=zeros(nnodes*6,nnodes*6);
globalrhs=zeros(nnodes*6,1);
```

```

% we will build elk and elf and immediately assemble

% start the big element loop

l=0;

%Alingment Index;

    for n=1:nem

        % zero elk and elf

        elk=zeros(24,24);

        % find the node numbers for this element

        i1=nod(n,1);

        i2=nod(n,2);

        i3=nod(n,3);

        i4=nod(n,4);

        % loop over the gauss points in xi/eta

        ngp=2;

        for gloopxi=1:ngp;

            for gloopeta=1:ngp;

                sf=zeros(4,1);

                dsf=zeros(4,2);

                gdsf=zeros(4,2);

                xi=gauss(gloopxi,ngp);

                eta=gauss(gloopeta,ngp);

                sf(1)=(1.0-xi)*(1.0-eta)/4;

                sf(2)=(1.0+xi)*(1.0-eta)/4;

```

```

sf(3)=(1.0+xi)*(1.0+eta)/4;
sf(4)=(1.0-xi)*(1.0+eta)/4;

% compute the xi and eta derives

dsf(1,1)=-1*(1.0-eta)/4.0;
dsf(2,1)=(1.0-eta)/4.0;
dsf(3,1)=(1.0+eta)/4.0;
dsf(4,1)=-1*(1.0+eta)/4.0;

dsf(1,2)=-1*(1.0-xi)/4.0;
dsf(2,2)=-1*(1.0+xi)/4.0;
dsf(3,2)=(1.0+xi)/4.0;
dsf(4,2)=(1.0-xi)/4.0;

% compute [j] at this gauss point;

jacmat=zeros(2,2);
jacmat(1,1)=x(i1).*dsf(1,1)+x(i2).*dsf(2,1)+x(i3).*dsf(3,1)+x(i4).*dsf(4,1);
jacmat(1,2)=x(i1).*dsf(1,2)+x(i2).*dsf(2,2)+x(i3).*dsf(3,2)+x(i4).*dsf(4,2);
jacmat(2,1)=y(i1).*dsf(1,1)+y(i2).*dsf(2,1)+y(i3).*dsf(3,1)+y(i4).*dsf(4,1);
jacmat(2,2)=y(i1).*dsf(1,2)+y(i2).*dsf(2,2)+y(i3).*dsf(3,2)+y(i4).*dsf(4,2);

% we have [j] at gauss point

jdet=jacmat(1,1).*jacmat(2,2)-jacmat(1,2).*jacmat(2,1);

% zero and fill j-inverse

jinv=zeros(2,2);

jinv(1,1)=jacmat(2,2)/jdet;

```

```
jinv(1,2)=-1*jacmat(1,2)/jdet;
```

```
jinv(2,1)=-1*jacmat(2,1)/jdet;
```

```
jinv(2,2)=jacmat(1,1)/jdet;
```

```
gdsf(1,1)=dsf(1,1).*jinv(1,1)+dsf(1,2).*jinv(2,1);
```

```
gdsf(2,1)=dsf(2,1).*jinv(1,1)+dsf(2,2).*jinv(2,1);
```

```
gdsf(3,1)=dsf(3,1).*jinv(1,1)+dsf(3,2).*jinv(2,1);
```

```
gdsf(4,1)=dsf(4,1).*jinv(1,1)+dsf(4,2).*jinv(2,1);
```

```
gdsf(1,2)=dsf(1,1).*jinv(1,2)+dsf(1,2).*jinv(2,2);
```

```
gdsf(2,2)=dsf(2,1).*jinv(1,2)+dsf(2,2).*jinv(2,2);
```

```
gdsf(3,2)=dsf(3,1).*jinv(1,2)+dsf(3,2).*jinv(2,2);
```

```
gdsf(4,2)=dsf(4,1).*jinv(1,2)+dsf(4,2).*jinv(2,2);
```

```
% at each G.P. add the contribution to and {elk}
```

```
for i=1:4;
```

```
    const=jdet.*weight(gloopxi,ngp).*weight(gloopeta,ngp);
```

```
    % elf(i)=elf(i)+sf(i)*const;
```

```
    for j=1:4;
```

```
        %k11
```

```
        elk(i,j)=elk(i,j)+(c11.*gdsf(i,1).*gdsf(j,1)+c16.*(gdsf(i,1).*gdsf(j,2)+gdsf(i,2).*gdsf(j,1))+c66.*gdsf(i,2).*gdsf(j,2)).*const;
```

```
        %k12
```

```
        elk(i,j+4)=elk(i,j+4)+(c12.*gdsf(i,1).*gdsf(j,2)+c16.*gdsf(i,1).*gdsf(j,1)+c26.*gdsf(i,2).*gdsf(j,2)+c66.*gdsf(i,2).*gdsf(j,1)).*const;
```

elk(j+4,i)=elk(i,j+4);

%k13

elk(i,j+8)=elk(i,j+8)+(e11.\*gdsf(i,1).\*gdsf(j,1)+e21.\*gdsf(i,1).\*gdsf(j,2)+e16.\*gdsf(i,2).\*gdsf(j,1)+e26.\*gdsf(i,2).\*gdsf(j,2)).\*const;

elk(j+8,i)=elk(i,j+8);

%k14

elk(i,j+12)=elk(i,j+12)+(d11.\*gdsf(i,1).\*gdsf(j,1)+d21.\*gdsf(i,1).\*gdsf(j,2)+d16.\*gdsf(i,2).\*gdsf(j,1)+d26.\*gdsf(i,2).\*gdsf(j,2)).\*const;

elk(j+12,i)=elk(i,j+12);

%k22

elk(i+4,j+4)=elk(i+4,j+4)+(c26.\*gdsf(i,1).\*gdsf(j,2)+c66.\*gdsf(i,1).\*gdsf(j,1)+c22.\*gdsf(i,2).\*gdsf(j,2)+c26.\*gdsf(i,2).\*gdsf(j,1)).\*const;

%k23

elk(i+4,j+8)=elk(i+4,j+8)+(e16.\*gdsf(i,1).\*gdsf(j,1)+e26.\*gdsf(i,1).\*gdsf(j,2)+e12.\*gdsf(i,2).\*gdsf(j,1)+e22.\*gdsf(i,2).\*gdsf(j,2)).\*const;

elk(j+8,i+4)=elk(i+4,j+8);

%k24

elk(i+4,j+12)=elk(i+4,j+12)+(d16.\*gdsf(i,1).\*gdsf(j,1)+d26.\*gdsf(i,1).\*gdsf(j,2)+d12.\*gdsf(i,2).\*gdsf(j,1)+d22.\*gdsf(i,2).\*gdsf(j,2)).\*const;

elk(j+12,i+4)= elk(i+4,j+12);

%k33

elk(i+8,j+8)=elk(i+8,j+8)+(-eps11.\*gdsf(i,1). \*gdsf(j,1)-eps12.\*gdsf(i,1). \*gdsf(j,2)-  
eps12.\*gdsf(i,2). \*gdsf(j,1)-eps22.\*gdsf(i,2). \*gdsf(j,2)).\*const;

%k34

elk(i+8,j+12)=elk(i+8,j+12)+(-g11.\*gdsf(i,1). \*gdsf(j,1)-g12.\*gdsf(i,1). \*gdsf(j,2)-  
g12.\*gdsf(i,2). \*gdsf(j,1)-g22.\*gdsf(i,2). \*gdsf(j,2)).\*const;

elk(i+12,j+8)=elk(i+8,j+12);

%k44

elk(i+12,j+12)=elk(i+12,j+12)+(-mu11.\*gdsf(i,1). \*gdsf(j,1)-  
mu12.\*gdsf(i,1). \*gdsf(j,2)-mu12.\*gdsf(i,2). \*gdsf(j,1)-mu22.\*gdsf(i,2). \*gdsf(j,2)).\*const;

%k55

elk(i+16,j+16)=elk(i+16,j+16)+(kxt.\*gdsf(i,1). \*gdsf(j,1)+kyt.\*gdsf(i,2). \*gdsf(j,2)).\*const;

%k66

elk(i+20,j+20)=elk(i+20,j+20)+(kxm.\*gdsf(i,1). \*gdsf(j,1)+kym.\*gdsf(i,2). \*gdsf(j,2)).\*const;

%k15

elk(i,j+16)=elk(i,j+16)+(-beta11.\*gdsf(i,1). \*sf(j)-beta12.\*gdsf(i,2). \*sf(j)).\*const;

%k16

elk(i,j+20)=elk(i,j+20)+(-zeta11.\*gdsf(i,1). \*sf(j)-zeta12.\*gdsf(i,2). \*sf(j)).\*const;

%k25

```

        elk(i+4,j+16)=elk(i+4,j+16)+(-beta12.*gdsf(i,1).*sf(j)-
beta22.*gdsf(i,2).*sf(j)).*const;

        %k26

        elk(i+4,j+20)=elk(i+4,j+20)+(-zeta12.*gdsf(i,1).*sf(j)-
zeta22.*gdsf(i,2).*sf(j)).*const;

        %k35

        elk(i+8,j+16)=elk(i+8,j+16)+(gamma1.*gdsf(i,1).*sf(j)+gamma2.*gdsf(i,2).*sf(j)).*const;

        %k36

        elk(i+8,j+20)=elk(i+8,j+20)+(gamma1.*gdsf(i,1).*sf(j)+gamma2.*gdsf(i,2).*sf(j)).*const;

        %k45

        elk(i+12,j+16)=elk(i+12,j+16)+(tau1.*gdsf(i,1).*sf(j)+tau2.*gdsf(i,2).*sf(j)).*const;

        %k46

        elk(i+12,j+20)=elk(i+12,j+20)+(nu1.*gdsf(i,1).*sf(j)+nu2.*gdsf(i,2).*sf(j)).*const;

        end

    end

end

end

```

```

% Rearranging the element matrices

q=[1 5 9 13 17 21 2 6 10 14 18 22 3    7 11 15    19 23 4 8 12
    16    20 24];

w=[1 5 9 13 17 21 2 6 10 14 18 22 3    7 11 15    19 23
4    8 12 16    20 24];

    elk=elk(w,q);

%{
for i=1:24
    for j=1:24
        globalk(i+l,j+l)=globalk(i+l,j+l)+elk(i,j);
    end
end
l=l+12;
%}

k=1;
for j=i1*6-5:i1*6
    j1(k)=j;
    k=k+1;
end

k=1;
for j=i2*6-5:i2*6

```

```

    j2(k)=j;
    k=k+1;
end

k=1;
for j=i3*6-5:i3*6
    j3(k)=j;
    k=k+1;
end

k=1;
for j=i4*6-5:i4*6
    j4(k)=j;
    k=k+1;
end

[A1,l]=sort([i1,i2,i4,i3]);
x1=[l(1)*6-5:l(1)*6];
x2=[l(2)*6-5:l(2)*6];
x3=[l(3)*6-5:l(3)*6];
x4=[l(4)*6-5:l(4)*6];

% we have {f} and {k} for element n

% assemble

```

```
globalk(j1,j1)=globalk(j1,j1)+elk(x1,x1);
globalk(j1,j2)=globalk(j1,j2)+elk(x1,x2);
globalk(j1,j3)=globalk(j1,j3)+elk(x1,x3);
globalk(j1,j4)=globalk(j1,j4)+elk(x1,x4);
globalk(j2,j1)=globalk(j2,j1)+elk(x2,x1);
globalk(j2,j2)=globalk(j2,j2)+elk(x2,x2);
globalk(j2,j3)=globalk(j2,j3)+elk(x2,x3);
globalk(j2,j4)=globalk(j2,j4)+elk(x2,x4);
globalk(j3,j1)=globalk(j3,j1)+elk(x3,x1);
globalk(j3,j2)=globalk(j3,j2)+elk(x3,x2);
globalk(j3,j3)=globalk(j3,j3)+elk(x3,x3);
globalk(j3,j4)=globalk(j3,j4)+elk(x3,x4);
globalk(j4,j1)=globalk(j4,j1)+elk(x4,x1);
globalk(j4,j2)=globalk(j4,j2)+elk(x4,x2);
globalk(j4,j3)=globalk(j4,j3)+elk(x4,x3);
globalk(j4,j4)=globalk(j4,j4)+elk(x4,x4);
```

```
end
```

```
% save the original [k] to solve for q's
```

```
oldglobalk=globalk;
```

```
oldrhs=globalrhs;
```

```

% For non-zero EBC's
u=zeros(nnodes*6,1);

for k=1:nabc;

    kk=nodebc(k);

    u(kk)=valebc(k);

end

globalrhs=-globalk*u;

for k=1:nabc;

    kk=nodnbc(k);

%    globalrhs(kk)=valnbc(k);

End

for k=1:nabc;

    kk=nodebc(k);

    for i=1:nnodes*6;

        globalk(i,kk)=0.0;

        globalk(kk,i)=0.0;

    end

    globalk(kk,kk)=1.0;

    globalrhs(kk)=valebc(k);

end

    u=globalk\globalrhs

%    q=oldglobalk*u;

%    Q=round(q*1000)/1000

```